Cell

Article

Assembly and activation of EBV latent membrane protein 1

Graphical abstract

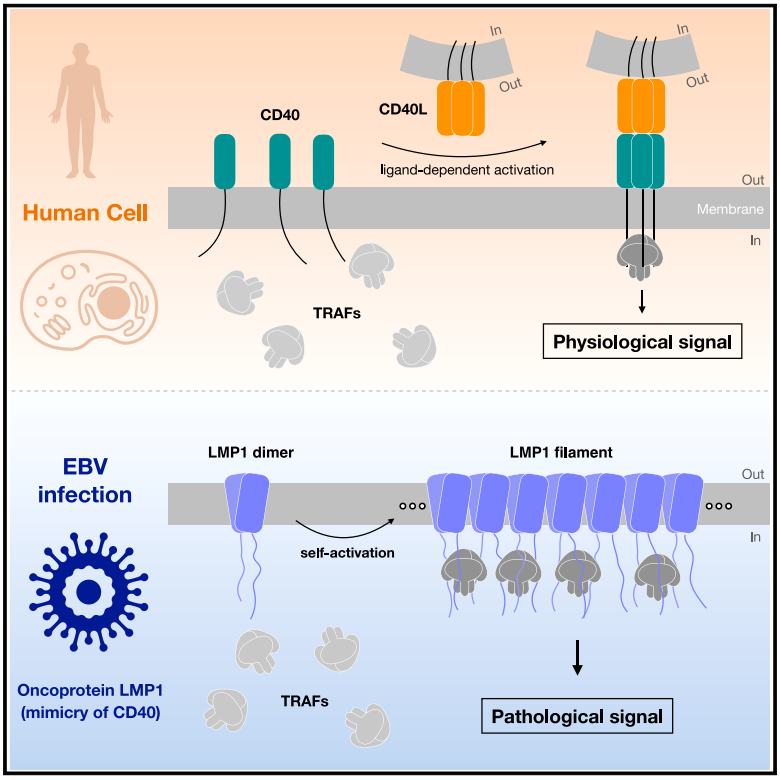

Highlights

- LMP1 adopts a non-canonical fold and forms a homodimer as its basic assembly unit
- LMP1 dimers further assemble side-by-side into higher-order filamentous oligomers
- Filamentous assembly of LMP1 allows efficient recruitment of downstream factors
- Disruption of higher-order assembly blocks LMP1-mediated signaling pathways

Authors

Jiafeng Huang, Xiaolin Zhang, Xiaohua Nie, ..., Liguo Zhang, Guangxia Gao, Pu Gao

Correspondence

liguozhang@ibp.ac.cn (L.Z.), gaogx@moon.ibp.ac.cn (G.G.), gaopu@ibp.ac.cn (P.G.)

In brief

LMP1, the primary oncoprotein of EBV, self-assembles into specific high-order filamentous oligomers that efficiently recruit downstream factors and induce pathogenesis.

Huang et al., 2024, Cell *187*, 4996–5009
September 5, 2024
https://doi.org/10.1016/j.cell.2024.06.021

CellPress

CellPress

Cell

Article

Assembly and activation of EBV latent membrane protein 1

Jiafeng Huang,[1,2,5] Xiaolin Zhang,[1,2,5] Xiaohua Nie,[1,2] Xuyuan Zhang,[1,2] Yong Wang,[1,2] Linlong Huang,[1,2] Xiaohan Geng,[2,3] Dong Li,[2,3] Liguo Zhang,[1,2,3,*] Guangxia Gao,[1,2,3,*] and Pu Gao[1,2,3,4,6,*]

[1]CAS Key Laboratory of Infection and Immunity, CAS Center for Excellence in Biomacromolecules, Institute of Biophysics, Chinese Academy of Sciences, Beijing 100101, China

[2]Key Laboratory of Biomacromolecules, Institute of Biophysics, Chinese Academy of Sciences, Beijing 100101, China

[3]University of Chinese Academy of Sciences, Beijing 100049, China

[4]Science and Technology Innovation Center, Shandong First Medical University, Shandong Academy of Medical Sciences, Jinan 250000, China

[5]These authors contributed equally

[6]Lead contact

*Correspondence: liguozhang@ibp.ac.cn (L.Z.), gaogx@moon.ibp.ac.cn (G.G.), gaopu@ibp.ac.cn (P.G.)

https://doi.org/10.1016/j.cell.2024.06.021

SUMMARY

Latent membrane protein 1 (LMP1) is the primary oncoprotein of Epstein-Barr virus (EBV) and plays versatile roles in the EBV life cycle and pathogenesis. Despite decades of extensive research, the molecular basis for LMP1 folding, assembly, and activation remains unclear. Here, we report cryo-electron microscopy structures of LMP1 in two unexpected assemblies: a symmetric homodimer and a higher-order filamentous oligomer. LMP1 adopts a non-canonical and unpredicted fold that supports the formation of a stable homodimer through tight and antiparallel intermolecular packing. LMP1 dimers further assemble side-by-side into higher-order filamentous oligomers, thereby allowing the accumulation and specific organization of the flexible cytoplasmic tails for efficient recruitment of downstream factors. Super-resolution microscopy and cellular functional assays demonstrate that mutations at both dimeric and oligomeric interfaces disrupt LMP1 higher-order assembly and block multiple LMP1-mediated signaling pathways. Our research provides a framework for understanding the mechanism of LMP1 and for developing potential therapies targeting EBV-associated diseases.

INTRODUCTION

Epstein-Barr virus (EBV) was the first human oncogenic virus discovered and causes a lifelong infection in approximately 95% of the world's population.[1–4] It is estimated that EBV accounts for up to 357,900 cases of cancer each year and 1.9% of the global cancer burden.[5] EBV infection leads to a variety of epithelial and lymphatic malignancies, including nasopharyngeal carcinoma, Burkitt lymphoma, Hodgkin lymphoma, natural killer (NK)/T cell lymphomas, leiomyosarcomas, and gastric cancer.[1,2,6–8] Central among the EBV-encoded factors that play regulatory roles in the malignant process is latent membrane protein 1 (LMP1), which has been recognized as the primary oncoprotein of the virus.[9,10] LMP1 is expressed in most EBV-associated lymphoproliferative diseases and malignancies and plays a critical role in the early development of EBV-mediated pathogenesis and disease phenotypes.[11–15] Extensive research has shown that LMP1 is essential for transformation and proliferation in multiple cell backgrounds *in vitro* as well as in transgenic mice.[14,16–19] As a pleiotropic factor, LMP1 has additional roles beyond cell transformation and immortalization, ranging from cytokine and chemokine induction, immune modulation, apoptotic resistance, cell migration, cell-cell contact, and invasive growth of cancer cells.[9,20–24] Given its central role in EBV-associated diseases, LMP1 is widely considered to be an ideal target for early differential diagnosis and targeted therapy.[6,14,23,25,26]

LMP1 is a functional analog of the CD40 costimulatory receptor with ligand-independent constitutive signaling activity.[27–29] The C-terminal flexible cytoplasmic tail of LMP1 harbors three C-terminal activation regions (CTAR1–3) to recruit tumor necrosis factor receptor (TNFR)-associated factors (TRAFs) or TNFR-associated death domain (TRADD) proteins, which in turn activate a variety of signaling cascades, including the nuclear factor-κB (NF-κB), c-Jun N-terminal kinase (JNK)/activator protein 1 (AP1), mitogen-activated protein kinase (MAPK), phosphatidylinositol 3-kinase (PI3K), and Janus kinase (JAK) pathways.[14,28–31] The diverse signaling activities and cellular functions of LMP1 are critically dependent on its N-terminal transmembrane domain, which is predicted to contain six transmembrane segments.[32] The transmembrane domain exhibits an intrinsic property to facilitate LMP1 oligomerization in the membrane, a feature that likely contributes

to the circumvention of ligand requirements and leads to the initiation of signal transduction at the C-terminal tail.[28] Several regions in the transmembrane domain have been proposed to be involved in intermolecular interaction, lipid raft localization, and immune suppression, and mutations or truncations of these regions result in disruption of LMP1 functions.[20,21,28,33–39]

Despite nearly four decades of research into the biological functions of LMP1, a fundamental understanding of LMP1 assembly and activation at the molecular level remains elusive, hampering efforts to develop potential therapeutics. In the current work, we applied an antibody-assisted strategy and determined high-resolution cryo-electron microscopy (cryo-EM) structures of LMP1 in both dimeric and higher-order oligomeric states. These structural findings, complemented by functional analyses, reveal many previously unanticipated mechanisms of LMP1 assembly and activation.

RESULTS

Structure determination of LMP1

Considering the central role of the transmembrane domain in mediating LMP1 membrane assembly and licensing downstream signaling, as well as the difficulties in sample preparation and structure determination caused by large flexible tails, we conducted most cryo-EM experiments using an LMP1 construct (residues 25–186; hereafter simply referred to as LMP1) with intact transmembrane domain and partial deletions of the N- and C-terminal tails (Figure S1A). Interestingly, size-exclusion chromatography (Figure S1B) and cryo-EM analysis (Figure S1C) for LMP1 reveal the existence of both dimeric and high-order oligomeric fractions, consistent with the previously proposed intrinsic oligomerization property of LMP1.[28] However, these cryo-EM data cannot provide high-resolution 3D reconstructions due to the small stable mass (only ~20 KDa) and lack of distinguishable soluble domains of LMP1. To facilitate cryo-EM reconstructions of LMP1, we performed systematic mouse immunization and antibody screening and successfully isolated a high-affinity antibody (Ab-4E9) showing rigid binding to LMP1 without affecting its oligomerization status (Figure S2). Using the antibody-assisted strategy, we were able to determine cryo-EM structures of LMP1 in its dimeric and oligomeric states at 3.5 Å resolution (Figures 1 and S3; Table S1). The quality of these electron density maps allows building of atomic models for LMP1 in both oligomerization states (Figure S4).

To confirm whether endogenous LMP1 from EBV-infected cells can still be recognized by the spatial epitope-selective antibody Ab-4E9, we first performed flow cytometry analysis using the widely used B95-8 cell line, an EBV-infected cell line established from peripheral blood lymphocytes. The results show a clear and dose-dependent antibody binding to LMP1 under both latent (in the absence of the inducer compound 12-O-tetradecanoylphorbol-13-acetate [TPA]) and activated (in the presence of TPA) EBV-infected physiological conditions (Figure S5A), similar to the positive control using a linear epitope-binding antibody (Ab-CTD: antibody specific for the C terminus of LMP1) targeting the disordered C-terminal region of LMP1 (Figure S5A). We further conducted immunofluorescence assays for Ab-4E9 in B95-8 cells and confirmed that endogenous LMP1 from EBV-infected cells can also form oligomerization and be recognized by this spatial epitope-selective antibody (Figure S5B). Together, these data suggest that endogenous LMP1 in EBV-infected cells is likely to adopt similar structures to those determined by cryo-EM.

Non-canonical fold of LMP1

The transmembrane domain of LMP1 contains six transmembrane segments (TM1–TM6) that are sequentially wrapped into a compact helix bundle in a counterclockwise direction when viewed from the extracellular side (Figure S6A). A large set of hydrophobic residues distributed along all six TMs face the interior of the protein to form a stable hydrophobic core (Figure S6A). The LMP1 monomer exhibits a roughly triangular prism shape to penetrate the cell membrane, with TM1/2/3/4, TM4/5, and TM1/5/6 forming the three cross sections, respectively (Figure S6A). Three short extracellular loops connect TM1–TM2/TM3–TM4/TM5–TM6 and contribute to the extremely small size of the extracellular exposed region (Figures S1A and S6A), a feature that is likely responsible for the poor immunogenicity and weak immune response of LMP1. In addition to the N- and C-terminal tails, LMP1 contains two intracellular loops connecting TM2–TM3 and TM4–TM5, with the second intracellular loop providing a major binding site for the antibody (Figures 1A and S1A). A Dali-server[40] search against all experimentally determined structures shows that LMP1 monomer represents a non-canonical fold for which no structural homolog has been reported. In addition, LMP1 differs significantly from the predicted models by AlphaFold2[41] in both overall structure and topology (Figures S6A–S6C), further highlighting the uniqueness of the LMP1 fold.

Assembly of LMP1 dimer

Since CD40, the functional analog of LMP1, and TRAFs, the downstream binding factors of LMP1 and CD40, both form a trimeric assembly to activate downstream signaling, it is reasonable to speculate that LMP1 also signals as a trimer.[27,30] Unexpectedly, our biochemical and structural results show that the basic assembly unit of LMP1 is actually a compact homodimer (Figures 2A and S1B). The overall structure of LMP1 dimer adopts a trapezoidal prism shape (Figure 2A), with an extracellular width of 32 Å, an intracellular width of 61 Å, and an overall thickness of 35 Å. The intracellular loops connecting TM4–TM5 are distributed away from the dimer interface so that the two bound antibodies do not interfere with dimer formation (Figure 2A). Similar to the LMP1 monomer, Dali-server[40] search and AlphaFold2[41] prediction show that the LMP1 dimer also represents a specific and unreported structural assembly (Figures S6D–S6F). The dimer is formed by a tight and antiparallel packing between the TM1/2/3/4 helices of each LMP1 monomer, with the two LMP1 subunits arranged in a 2-fold symmetric manner (Figure 2A). The dimer interface covers a large buried area of ~1,986 Å^2 (Figures S7A and S7B), where intermolecular binding is dominated by hydrophobic interactions and further strengthened by a hydrogen bond (Figures 2B and 2C). The 2-fold symmetry roughly divides the LMP1 dimer interface into three, four-helix bundles, one of which involves TM2/TM3 helices from both subunits with the 2-fold axis in the center (Figures 2A and 2B), and the other two are symmetrically related

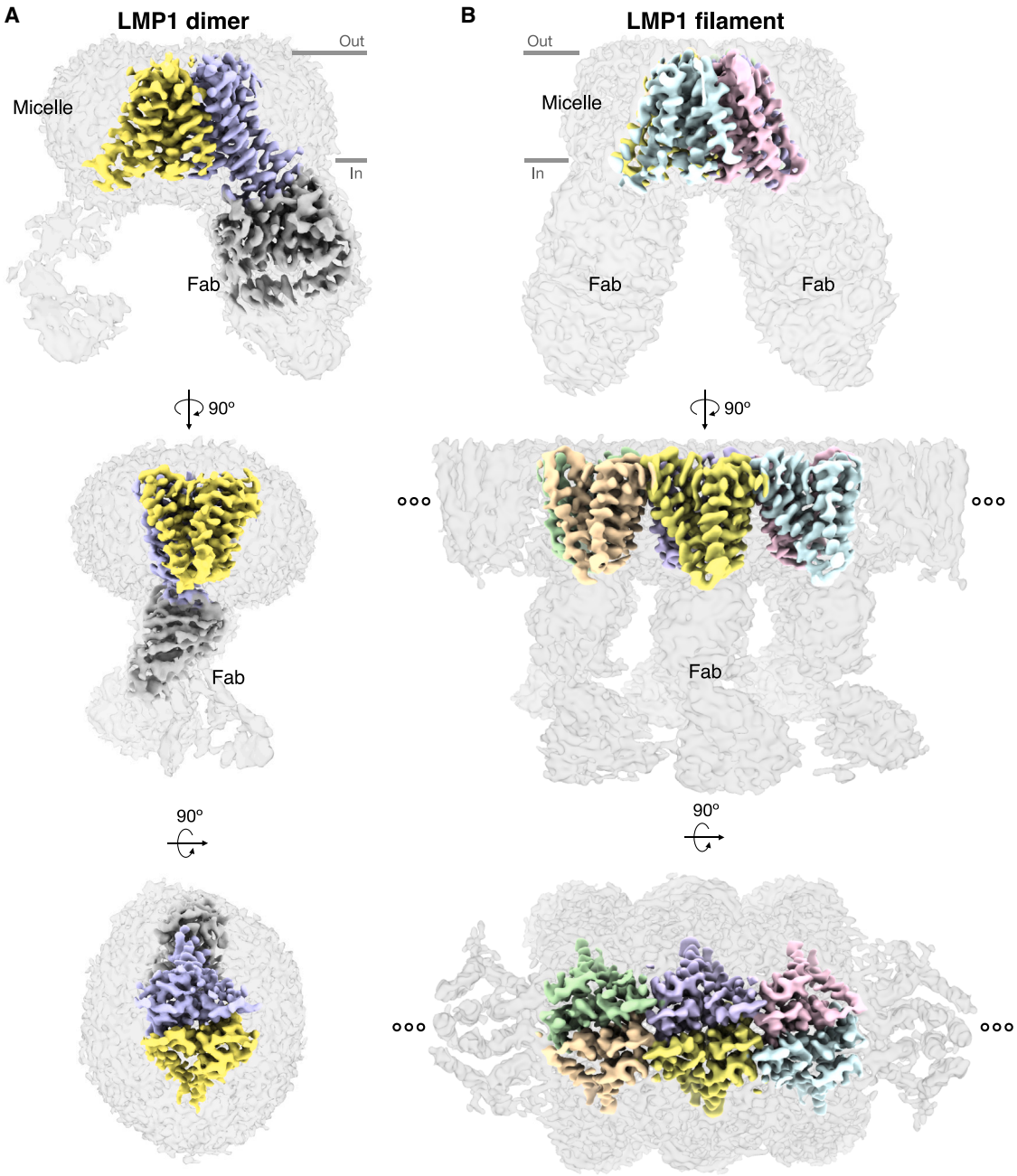

Figure 1. Cryo-EM structures of LMP1 dimer and oligomer

Three views of the cryo-EM 3D reconstruction of LMP1 dimer-Fab complex (A) and LMP1 filament-Fab complex (B), with low contour level in gray and high contour level in color. The micelle is presented as semi-transparent surface. The two subunits in the dimer are colored in yellow and blue. The Fab is colored in silver. The core subunits in the filament are colored in beige, green, yellow, blue, pink, and cyan. The formation of the higher-order oligomers is mediated by the side-by-side packing of LMP1 dimer.

See also Figures S1, S2, S3, S4, S5, and S6 and Table S1.

and involve TM3/TM4 from one LMP1 and TM1/TM2 from the other (Figures 2A and 2C). The strong inter-subunit contacts and the symmetrical subunit arrangement together ensure a stable dimeric assembly unit of LMP1 and rule out the possibility of LMP1 trimer formation.

To evaluate the importance of LMP1 dimer interface, we conducted cellular experiments to assess the effects of interface mutants (Table S2) on LMP1-mediated NF-κB pathway activation. Specifically, the alanine or serine substitutions of selected residues in different regions (dimer_mut1, dimer_mut2,

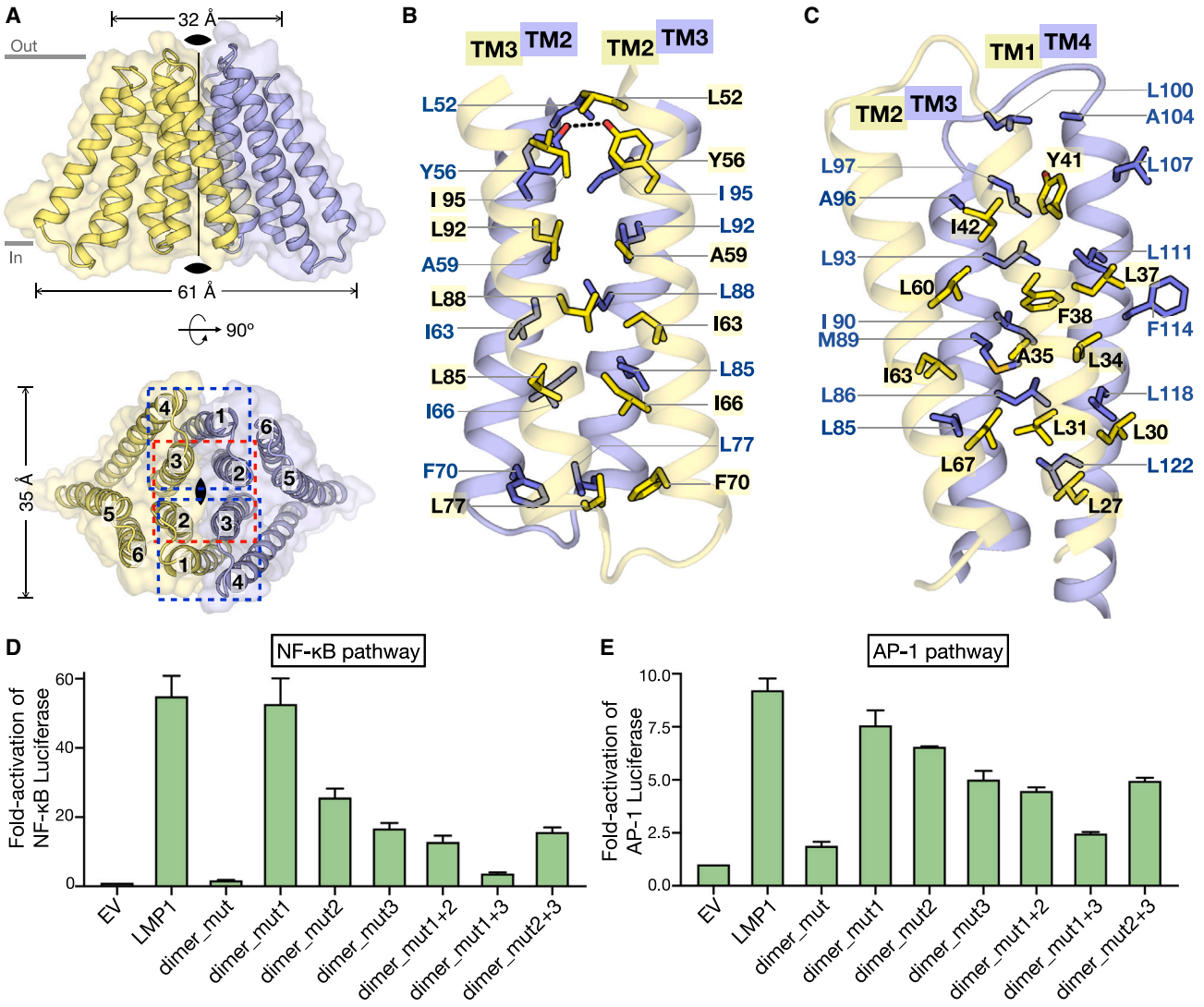

Figure 2. Assembly of LMP1 dimer

(A) Side and top views of LMP1 dimer. The two subunits in the dimer are colored in yellow and blue. Three four-helix bundles are marked by dashed boxes.

(B and C) The intermolecular contacts mediated by TM2/3-TM2/3 (B) and TM1/2-TM3/4 (C). TM2/3-TM2/3 (B) represents the four-helix bundle highlighted by the red dashed box in (A). TM1/2-TM3/4 (C) represents one of the two similar four-helix bundles highlighted by blue dashed boxes in (A). Residues in the hydrophobic cavity are shown in stick representation. Intermolecular binding is mainly contributed by hydrophobic interactions. The hydrogen bond is shown in black dash line.

(D and E) Effects of LMP1^{fl} mutations in the dimer interface on LMP1-induced activation of the NF-κB pathway (D) and JNK/AP1 pathway (E). Averages and error bars of fold induction in luciferase assay are based on three independent experiments. Data are represented as mean ± SD.

See also Figures S3, S4, S6, and S7 and Table S2.

dimer_mut3, dimer_mut4, dimer_mut5) lead to different effects on LMP1-mediated NF-κB signaling, with a marked reduction for dimer_mut2, dimer_mut3, dimer_mut4, dimer_mut5, and a very minor effect for dimer_mut1 (Figures 2D, S7C, and S7D). The combinations of mutations (dimer_mut1+2, dimer_mut1+3, dimer_mut2+3) lead to more significant effects on NF-κB signaling activity (Figures 2D and S7C). Interestingly, although dimer_mut1 alone barely reduces signaling activity (Figure 2D), its combinations with other mutants notably enhance their reduction efficiencies (Figure 2D). Furthermore, a relatively more complete mutant covering the entire dimer interface (dimer_mut) practically abolishes LMP1-mediated NF-κB activation (Figure 2D) and behaves as a monomer (Figure S1B). In addition to NF-κB signaling, these dimer interface mutations also result in similar reduction effects on LMP1-mediated activation of JNK/AP1 signaling (Figures 2E, S7C, and S7D), further suggesting a conserved role for the LMP1 dimer assembly. Taken together, our structural and functional data demonstrate the specific assembly of LMP1 dimer and its critical role in LMP1 function.

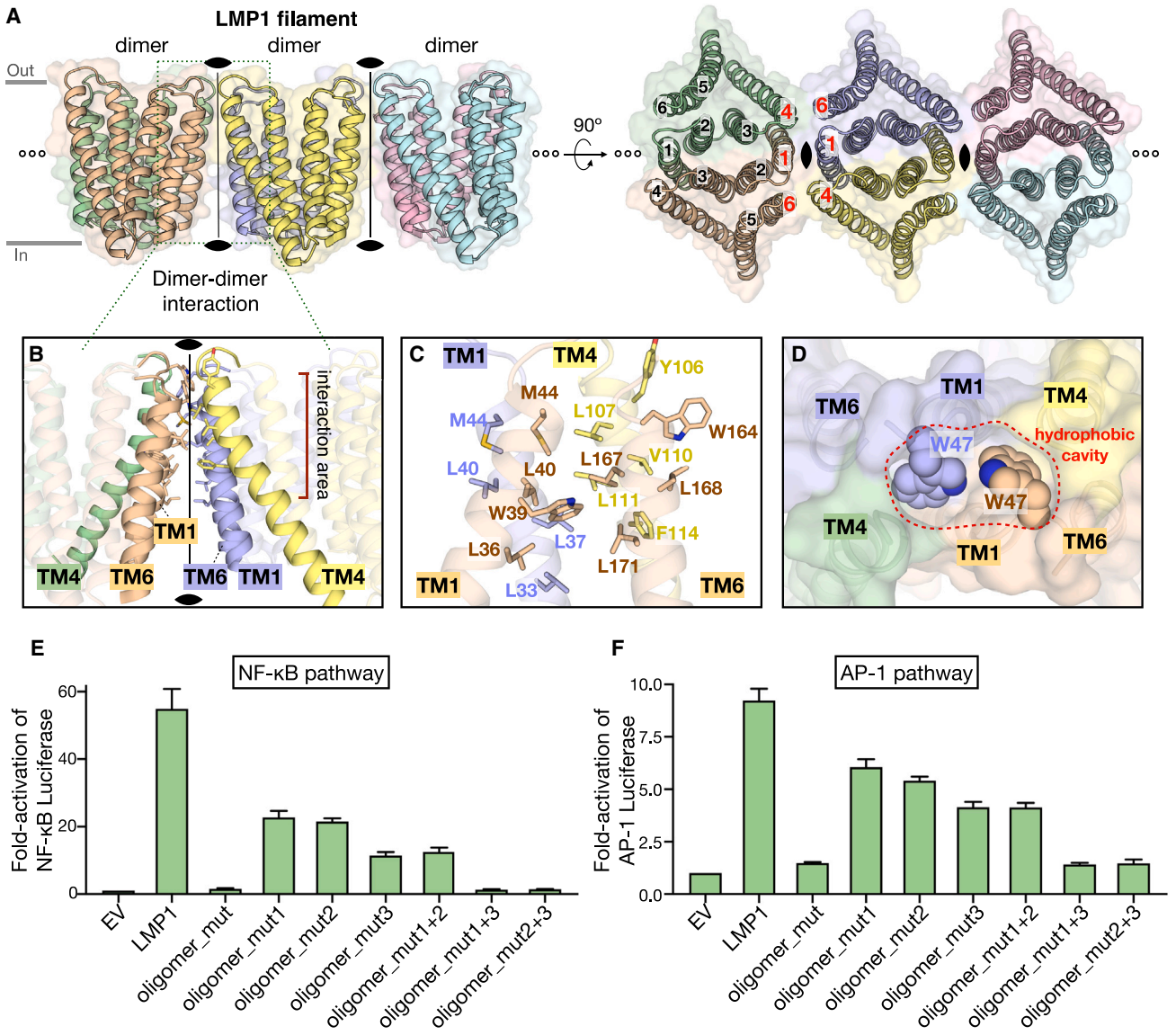

Figure 3. Assembly of LMP1 oligomer

(A) Side and top views of LMP1 oligomer. The subunits are colored in beige, green, yellow, blue, pink, and cyan. The higher-order oligomers are mediated by the side-by-side packing of TM4/TM1/TM6 helices.

(B) Side view of LMP1 oligomer interface. Zoom in on the dashed box in (A).

(C) Detailed interactions within the four-helix bundle of LMP1 oligomer interface, containing one TM4, one TM6, and two TM1. Intermolecular binding is mainly contributed by hydrophobic interactions. Residues in the hydrophobic cavity are shown in stick representation.

(D) Two W47 residues (space-filling) from the extracellular TM1-TM2 loops of adjacent LMP1 dimers (cartoon) bind within the hydrophobic pockets of the oligomeric interface (surface).

(E and F) Effects of LMP1^{fl} mutations in the oligomer interface on LMP1-induced activation of the NF-κB pathway (E) and JNK/AP1 pathway (F). Averages and error bars of fold induction in luciferase assay are based on three independent experiments. Data are represented as mean ± SD.

See also Figures S3, S4, and S7 and Table S2.

Assembly of LMP1 oligomer

Intriguingly, LMP1 assembles into unexpected higher-order filament oligomers that are organized by linear side-by-side stacking of adjacent LMP1 dimers (Figures 1B, 3A, S1C, and S2C). To form this filament architecture, each LMP1 dimer contributes two symmetrically related regions on either side containing TM1/TM4/TM6 helices, where TM4 comes from one LMP1 subunit and TM1/TM6 from the other (Figure 3A). The oligomeric interface buries an area of ~1,044 Å^2 and is primarily mediated by hydrophobic contacts between the extracellular halves of two TM1/TM4/TM6 regions from adjacent LMP1 dimers (Figures 3A and 3B). The other parts of these two regions stand apart from each other, thereby creating a hydrophobic cavity between LMP1 dimers near the intracellular side (Figures 3A and

3B). The assembly mode of LMP1 oligomer and the existing 2-fold symmetry within LMP1 dimer ensure an interdimer 2-fold symmetry (Figures 3A and 3B), which then divides the oligomeric interface into two symmetrically related four-helix bundles, each containing one TM4, one TM6, and two TM1 (Figures 3A and 3C). Several hydrophobic residues together contribute to the core of the four-helix bundle (Figure 3C), specifically Y106/L107/V110/L111/F114 from TM4, W164/L167/L168/L171 from TM6, L36/W39/L40/M44 from one TM1, and L33/L37/L40/M44 from the other TM1. In addition to the contacts formed by transmembrane helices, the LMP1 filament assembly is further strengthened by two tryptophan residues (W47) from the extracellular TM1–TM2 loops of adjacent LMP1 dimers, which perfectly fill the hydrophobic grooves of the two, four-helical bundles from the extracellular side (Figure 3D). Structural superimposition shows that there are no significant overall conformational differences between the isolated LMP1 dimer and the LMP1 dimer in an oligomer, with a main chain Cα root mean standard deviation (RMSD) of 0.7 Å (Figure S4C). The only notable movement is the extracellular loop connecting TM1–TM2, which facilitates the W47 residue (Figure S4C) to form the hydrophobic interactions within oligomeric interfaces (Figure 3D).

To validate whether this filament assembly is critical for LMP1's functions, we introduced different mutations (Table S2) to the oligomeric interface and assessed their effects on LMP1-mediated signaling activation of both NF-κB and JNK/AP1 pathways. Compared with the wild-type (WT) protein, five mutants covering different interface regions (oligomer_mut1, oligomer_mut2, oligomer_mut3, oligomer_mut4, and oligomer_mut5) all lead to a significant reduction in LMP1-mediated NF-κB and JNK/AP1 signaling (Figures 3E, 3F, S7C, and S7D). The combinations of these mutations (oligomer_mut1+2, oligomer_mut1+3, oligomer_mut2+3) cause more dramatic effects on the signaling activities (Figures 3E and 3F). As expected, a more extensive mutation of the oligomeric interface (oligomer_mut) also virtually eliminates LMP1-mediated signaling (Figures 3E and 3F). Moreover, LMP1 oligomeric interface mutants show similar patterns of effects on activation of both NF-κB and JNK/AP1 pathways (Figures 3E, 3F, and S7D), suggesting the conserved importance of this filamentous assembly for multiple functions mediated by LMP1.

To confirm whether the representative LMP1 mutants still cause signaling reductions in the more physiological lymphoid cells, we measured LMP1-mediated NF-κB pathway activation for WT, dimer_mut, and oligomer_mut using the B lymphoblast Daudi cell line (Figures S7E and S7F). It should be noted that the expression levels of WT and mutant LMP1 in Daudi cells are well within the physiological levels of EBV-infected B95-8 cells (Figure S7F). The results clearly confirm that the dimeric and oligomeric interface mutants, identified from cryo-EM structures and validated in HEK293 cells (Figures 2 and 3), also have similar effects in established lymphoid cells.

LMP1 oligomer formation in cells

To further complement the biochemical (Figures S1B and S2A), structural (Figures 1B and 3A), and functional (Figures 3E and 3F) evidence for the oligomeric assembly of LMP1, we conducted direct cellular imaging analysis for LMP1 and its mutants. In addition to the mutants targeting our newly identified dimeric (dimer_mut) and oligomeric (oligomer_mut) interfaces, we also included a previously well-studied mutant of the FWLY motif (residues F38-W39-L40-Y41) in TM1 (38-FWLY-41 to 38-AALA-41; termed LMP1^{AALA}). The FWLY motif has been proposed to contribute to lipid raft localization of LMP1, and the LMP1^{AALA} mutation has significant effects on LMP1 signaling.[23] Our structural results provide a detailed molecular explanation for the function of the FWLY motif and show that this motif plays an important role in the dimer and oligomer assembly of LMP1, with F38 and Y41 buried in the dimer interface and W39 and L40 in the oligomer interface (Figure S8A). Our cellular functional assays further confirm that the LMP1^{AALA} mutation significantly reduces LMP1-mediated NF-κB pathway activation (Figure S8B). We first performed confocal fluorescence microscopy experiments with HeLa cells expressing the GFP-tagged WT LMP1 or its mutants. The results show that WT LMP1 forms higher-order membrane puncta structures (Figure 4A) similar to the previously reported subcellular localization pattern,[42] whereas this oligomerization phenotype is largely abolished for the three mutants (dimer_mut, oligomer_mut, LMP1^{AALA}) that affect dimer or oligomer assembly (Figure 4A).

We then applied total internal reflection fluorescence (TIRF)-structured illumination microscopy (SIM) to better visualize the nanoscale organization of LMP1 membrane assemblies in living specimens using HeLa cells expressing WT or mutant LMP1 (Figures 4B–4D). The TIRF-SIM super-resolution imaging results clearly show that WT LMP1 assembles into linear clusters on the membrane with dimensions ranging from ∼125 to ∼1,250 nm (Figures 4C and 4D), whereas all three mutants show a relatively homogeneous distribution of small dots (Figure 4B). These linear clusters of WT protein likely correspond to the higher-order puncta structures by confocal microscopy (Figure 4A) and the filament oligomers by cryo-EM (Figures 1B and S3D–S3F), while the small dots of the mutants may represent non-oligomeric individual LMP1 dimers or monomers (Figure 4B). To compare the differences in a more quantified manner, we generated a length-based distribution plot for each identified LMP1 cluster or dot and again confirmed that the three mutants form significantly smaller assemblies than the WT protein in living cells (Figure 4E). Given that each LMP1 dimer occupies a length of ∼35 Å in the filament assembly (Figure 4F), the cellular clusters observed by TIRF-SIM are thus composed of ∼35–350 repeats of LMP1 dimers (Figures 4C–4E). In summary, super-resolution microscopy analysis confirms that LMP1 forms nanometer-scale filaments in living cells and that both intra- and inter-dimer interfaces are critical for this cellular oligomerization.

To determine whether concentration is a key factor for LMP1 oligomerization, we generated cell lines with inducible and controllable LMP1 expression within the physiological levels of EBV-infected B95-8 cells (Figure S7G). Using these cell lines, we systematically measured the filament formation and filament length distribution of LMP1 at different expression levels. The results show that LMP1 does indeed form more oligomers as more protein is produced in the cell and that the lengths of LMP1 oligomers will also increase as the protein expression level increases (Figures 5A and 5B). Although these results clearly demonstrate

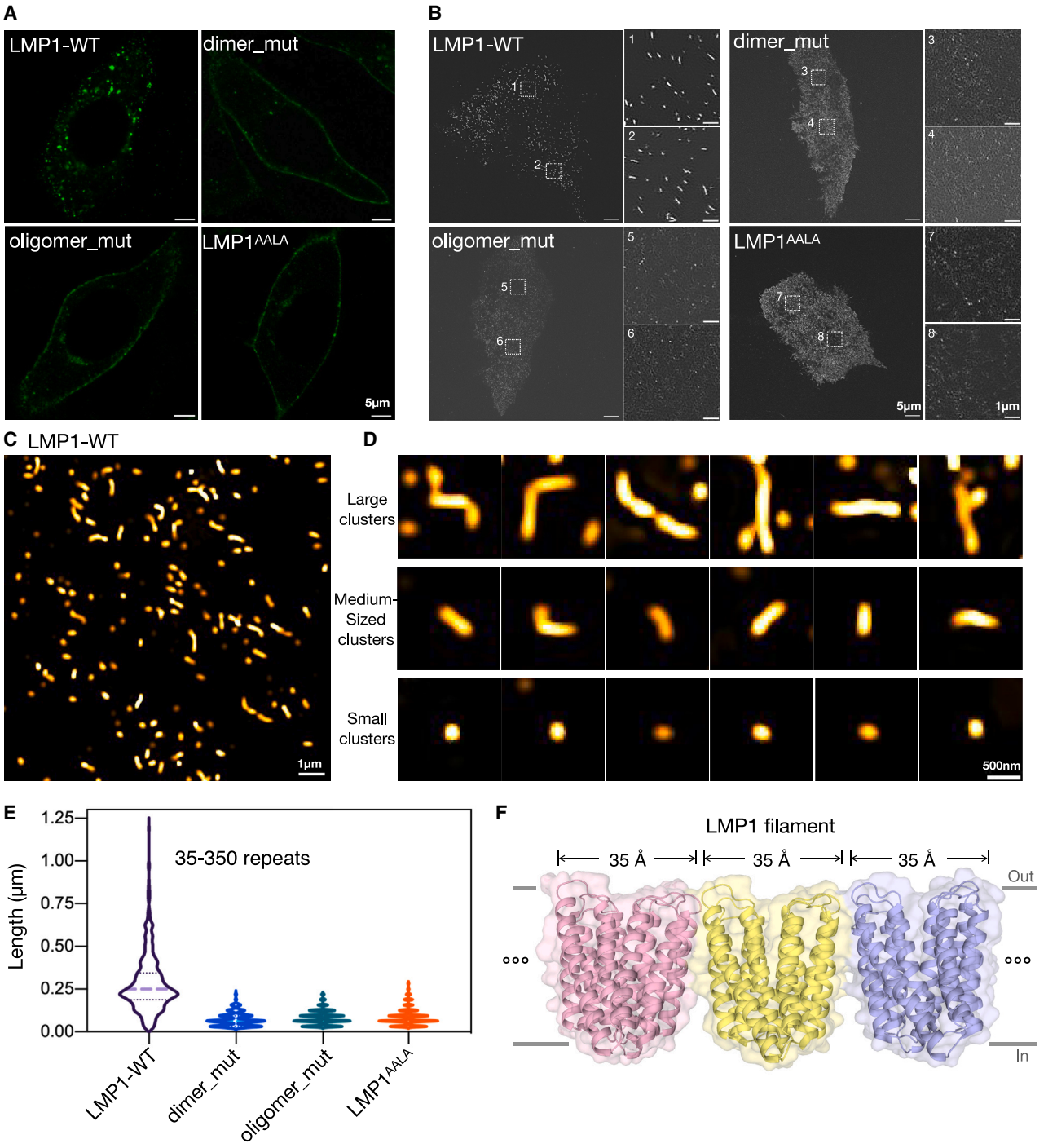

Figure 4. Super-resolution imaging of LMP1 assemblies

(A) Confocal imaging of HeLa cells expressing GFP-LMP1^{fl}, GFP-dimer_mut, GFP-oligomer_mut, and GFP-LMP1^{AALA}. Scale bars, 5 μm.

(B) TIRF-SIM super-resolution imaging of GFP-LMP1^{fl} and mutants in cells from (A) using TIRF illumination of the basal plane. Scale bars, 5 μm. The indicated outlined regions are magnified on the right of each image. Scale bars, 1 μm.

(C) Overview SIM reconstruction of assemblies in HeLa cells expressing GFP-LMP1^{fl} including filamentous structures. Scale bars, 1 μm.

(D) Gallery of GFP-LMP1^{fl} clusters found in HeLa cells. Scale bars, 500 nm. All the data are representative of at least three independent experiments.

(E) Length of the filaments for each identified GFP-LMP1^{fl} cluster. Violin plots show the distribution of all identified clusters. Lines indicate median values. The LMP1-WT clusters are composed of ~35–350 repeats of LMP1 dimers.

(F) The overall thickness of one LMP1 dimer in LMP1 filament is ~35 Å.

See also Figure S8.

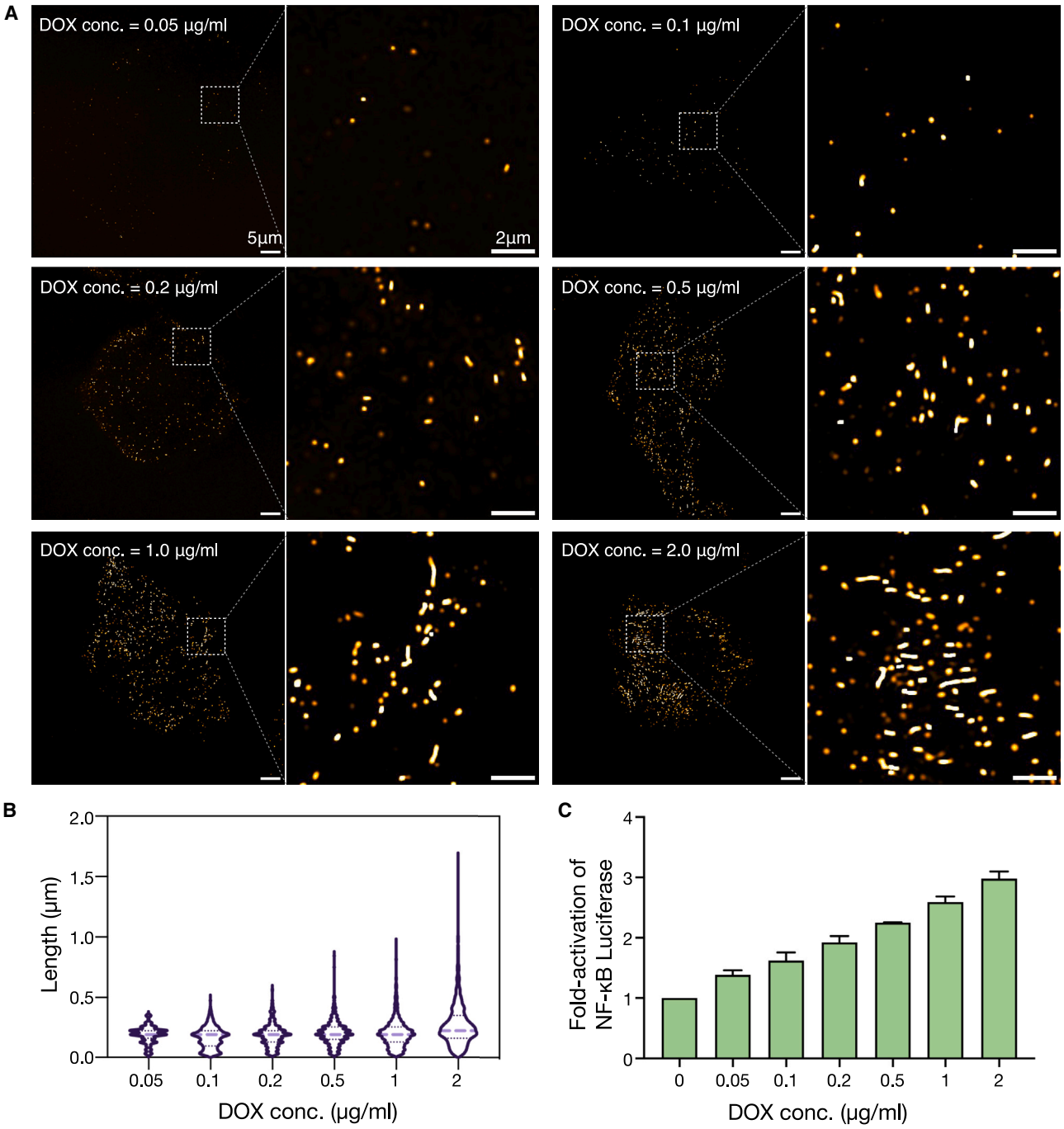

Figure 5. Concentration-dependent assembly and activation of LMP1

(A) TIRF-SIM super-resolution imaging of different concentrations of GFP-LMP1^{fl} in HeLa cells. Scale bars, 5 µm. The indicated outlined regions are magnified on the right of each image. Scale bars, 2 µm.

(B) Violin plots show the distribution of all identified clusters. Lines indicate median values.

(C) Concentration-dependent activation of GFP-LMP1^{fl} on LMP1-induced activation of the NF-κB pathway. Averages and error bars of fold induction in luciferase assay are based on three independent experiments. Data are represented as mean ± SD.

See also Figure S7.

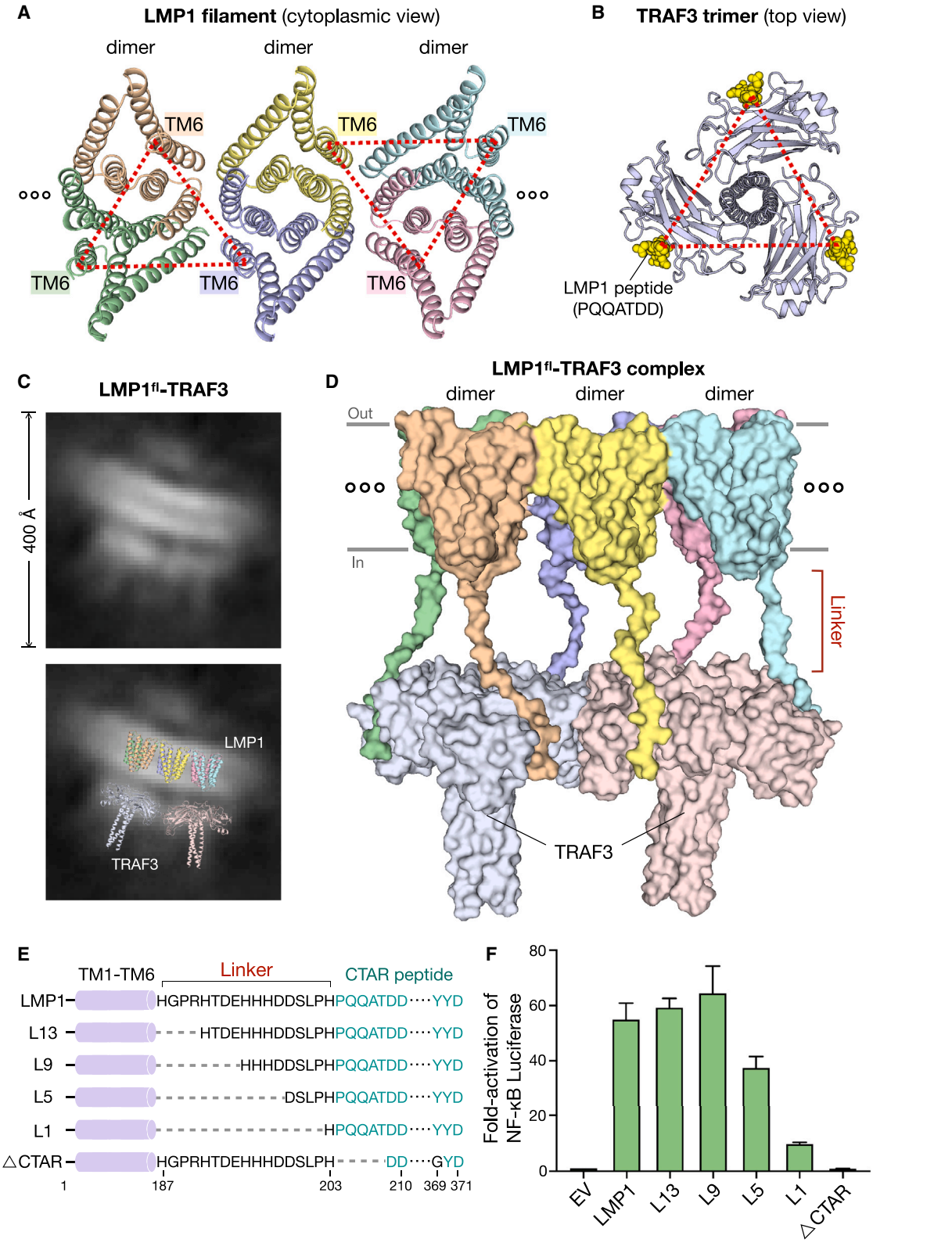

(legend on next page)

a relationship between protein concentration and activation, there is no sharp concentration threshold for oligomerization and activation (Figure 5B). Moreover, LMP1 still forms oligomers at lower expression levels, albeit of relatively shorter length (Figure 5B). In line with the results of filament formation and filament length distribution, the degree of LMP1-mediated NF-κB pathway activation also shows a similar pattern (Figure 5C).

Oligomerization promotes LMP1 signaling activity

In contrast to CD40, which relies on ligand-induced trimerization to recruit downstream TRAFs, LMP1 exhibits ligand-independent constitutive signaling activity. Our structural and functional results show that LMP1 forms a dimer rather than a trimer as its basic assembly unit (Figure 2) and that filamentous oligomerization of LMP1 dimer is critical for downstream signaling activity (Figure 3). Interestingly, the filamentous assembly of LMP1 ensures a roughly equilateral triangular distribution for the TM6 C terminus of two LMP1 subunits from one dimer and another LMP1 subunit from the adjacent dimer (Figure 6A). Thus, the self-association of LMP1 oligomer results in a cluster of such ''pseudo-trimers'' (Figure 6A), which can readily recruit multiple TRAF trimers for signaling activation (Figure 6B). To better understand how the LMP1 oligomer recruits TRAFs, we biochemically reconstituted a complex of full-length LMP1 carrying the entire CTAR regions and a TRAF3 construct (aa 313–504) with intact LMP1 binding region (Figure S8C). The stoichiometry of LMP1 to TRAF is approximately 0.9:1 based on the quantified bands on SDS-PAGE gel (Figure S8C). Although cryo-EM analysis of the LMP1-TRAF3 complex cannot provide a reliable 3D reconstruction due to the intrinsic flexibility of the sample, the 2D class average results show a clear projection of LMP1 oligomer bound to multiple TRAF3 trimers (Figure 6C). Based on the 2D class average of LMP1-TRAF3 complex (Figure 6C), the cryo-EM structure of LMP1 filament (Figure 6A), as well as the crystal structure of TRAF3 trimer bound to the CTAR1 peptide (Figure 6B) (PDB: 1ZMS),[43] we were able to build a structural model of LMP1 filament bound to TRAF3 trimers with no steric hindrance (Figures 6C and 6D). According to this model, three adjacent LMP1 dimers can recruit up to two TRAF3 trimers (Figure 6D), with the three CTAR1 peptides from each LMP1 pseudo-trimer (Figure 6A) perfectly occupying the three pockets of a TRAF3 trimer (Figure 6B). There is a 17-aa linker between TM6 and CTAR1, which likely plays a role in providing the necessary flexibility and coordinating an easy docking between LMP1 and TRAF3 (Figures 6D and 6E). By introducing various deletions into this flexible linker, we observed a gradual reduction in LMP1-mediated NF-κB signaling once the linker is shorter than nine residues, confirming the important role of this region (Figures 6F and S8D). Taken together, these data suggest a working model in which the higher-order filamentous assembly of LMP1 provides a robust signaling platform for recruitment of downstream factors and promotion of ligand-independent constitutive activation.

DISCUSSION

Despite extensive research on the biological functions of LMP1 and its primary contribution to EBV-derived pathogenesis, the molecular basis for LMP1 folding, assembly, and activation remains unclear. Structural resolution of LMP1 in both dimeric and oligomeric states serves as a framework for understanding the molecular mechanism of LMP1's functions. Interestingly, unlike its functional analog CD40 that relies on ligand-triggered trimerization for signaling activation (Figure 7A), LMP1 adopts a stable and symmetric homodimer as its basic assembly unit (Figure 7B). Since TRAF proteins, the downstream factors of both CD40 and LMP1, signal as trimers and contain three symmetrical LMP1 or CD40 binding pockets, the dimeric assembly of LMP1 results in a mismatch with TRAF trimers. To solve this problem, multiple LMP1 dimers are further assembled side-by-side into linear filamentous oligomers (Figure 7B). In this way, the transmembrane domain-mediated oligomerization of LMP1 licenses the accumulation of multiple flexible cytoplasmic tails that harbor TRAF-binding regions, thereby enabling an efficient recruitment of TRAFs and robust activation of downstream signaling (Figure 7B). Moreover, the filamentous assembly of LMP1 arranges an approximately equilateral triangular distribution for the cytoplasmic tails from adjacent LMP1 dimers, further facilitating recognition between the symmetric TRAF trimer and LMP1 (Figures 6A–6D). The ligand-independent self-association ability and the large number of LMP1 molecules in each higher-order oligomer allow LMP1 to induce very potent downstream signaling in a constitutive and ligand-independent manner (Figure 7B). Our model is supported by previous reports that a chimeric protein linking the cytoplasmic tail of CD40 to the transmembrane domain of LMP1 shows much stronger signaling activity than the original CD40.[29,44]

The cryo-EM structures of LMP1 in different oligomeric states also provide accurate explanations for the functions of previously studied LMP1 variants and mutants. A well-characterized TM1–TM4 deleted variant of LMP1, termed lytic LMP1, is highly

Figure 6. Structure model of full-length LMP1 bound to TRAF3

(A) Structure of LMP1 filament, highlighting the roughly equilateral triangular distribution for the TM6 C terminus.

(B) Structure of the TRAF3 trimer bound to LMP1 peptides (PDB: 1ZMS). LMP1 peptides are shown in sphere representation and colored in yellow.

(C) Representative cryo-EM 2D class averages of $LMP1^{fl}$-TRAF3 (upper) and the superimposition between cryo-EM 2D class averages with atomic structures (lower).

(D) Structural model of $LMP1^{fl}$-TRAF3 complex based on the 2D class average of $LMP1^{fl}$-TRAF3 complex, the cryo-EM structure of LMP1 filament, as well as the crystal structure of TRAF3 trimer bound to the CTAR1 peptide (PDB: 1ZMS).

(E) Truncations of the linker between TM region and C-terminal activation region.

(F) Effects of linker truncations and CTAR1 deletion on LMP1-induced activation of the NF-κB pathway. Averages and error bars of fold induction in luciferase assay are based on three independent experiments. Data are represented as mean ± SD.

See also Figure S8.

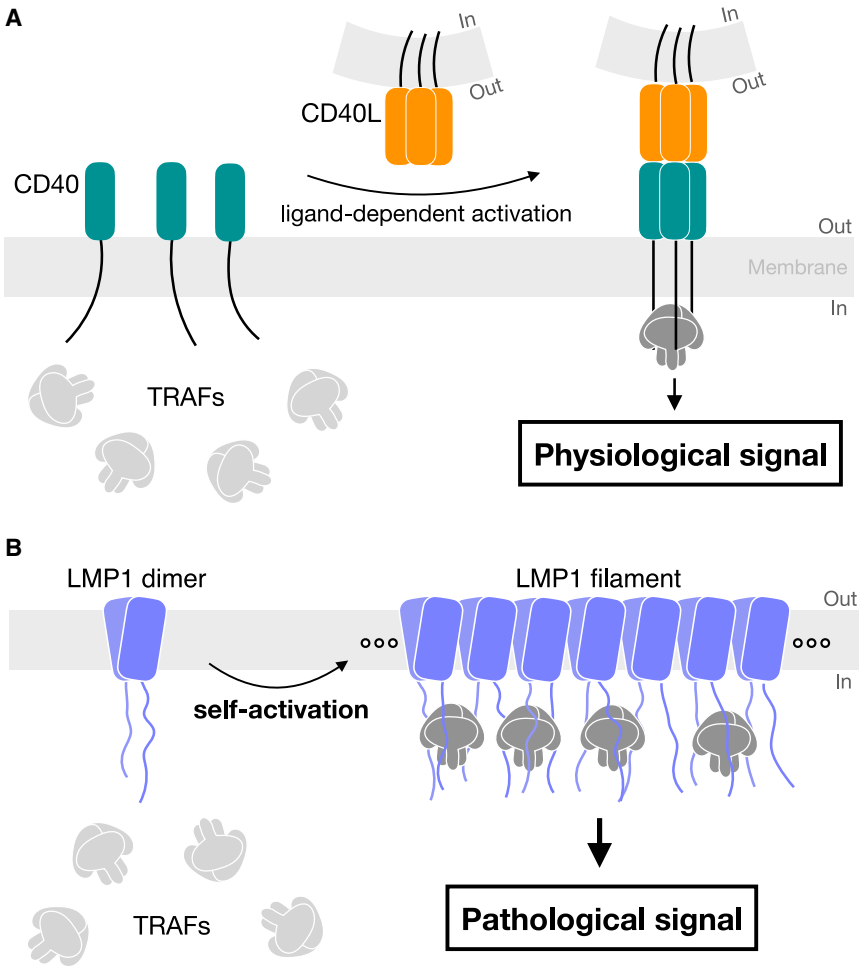

Figure 7. Different activation modes of CD40 and LMP1

(A) CD40L induces the trimerization of CD40, which then recruits TRAF trimers and activates downstream physiological signaling.

(B) LMP1 dimer self-assembles and rearranges into higher-order filament structures, which then more efficiently recruit multiple TRAF trimers and cause pathological signaling, potentially leading to oncogenesis.

See also Figures S1, S2, S3, and S4.

expressed during the lytic cycle of EBV infection and shows no transforming activity in cells.[28,38,45,46] We now understand that the absence of TM1–TM4 would completely disrupt the monomer folding, dimer formation, and oligomer assembly of LMP1, thereby blocking the downstream signaling. Interestingly, lytic LMP1 has also been shown to inhibit the activity of full-length LMP1,[37] likely by promoting the degradation of full-length LMP1.[47,48] In addition, TM3–TM6 and the FWLY motif in TM1 (38-FWLY-41) have been proposed to form intermolecular interactions and mediate LMP1 oligomerization and signaling.[34,35] The cryo-EM structures provide a direct explanation for which residues are involved in intra- and inter-dimer interactions and how TM3–TM6 and the FWLY motif contribute to oligomer assembly. Moreover, although the FWLY motif has also been implicated in lipid raft localization of LMP1,[33,34] this motif is completely buried within the dimer and oligomer interfaces and may indirectly facilitate lipid raft localization through mediating LMP1 oligomerization.

In addition to promoting a better mechanistic understanding of LMP1's functions, the current work also provides insights for potential therapeutic development against EBV-associated diseases. Given that the newly identified dimer and oligomer interfaces are both critical for LMP1-mediated signaling, the development of specific small molecules or peptides that interfere with dimer or oligomer assembly would be a specific and effective strategy. Moreover, considering the relatively smaller buried area of the oligomer interface, the design of specific therapeutics that target oligomer assembly may be a more feasible approach. The extremely small extracellular exposed region of LMP1 may contribute to poor immunogenicity and weak antibody responses, reminiscent of the demonstrated evolutionary feature of LMP1 to avoid T cell responses.[25,49,50] The dimer and oligomer assemblies increase the extracellular region of LMP1 and thus may provide new binding epitopes for the generation and design of extracellular antibodies against LMP1. Besides serving as an ideal target for differential diagnosis and targeted therapy, ectopically expressed LMP1 in patient tumor B cells has also been developed as a tool to promote the rapid production of autologous cytotoxic $CD4^+$ T cells for treating B cell malignancies.[25] A better understanding of the molecular basis of assembly and activation may also contribute to the next generation of LMP1-based applications.

In summary, our work provides detailed information for understanding the molecular mechanisms of folding, assembly, and activation of the EBV-encoded primary oncoprotein LMP1. This work may also serve as an important reference for the development of effective therapies targeting EBV-associated diseases.

Limitations of the study

Our study provides insight into the assembly and activation mechanisms of the EBV oncoprotein LMP1; however, two major limitations remain. First, although LMP1 has been proposed to associate with lipid rafts, the predicted lipid raft anchoring motif (38-FWLY-41) is completely buried within the dimer and oligomer interfaces rather than directly facing the lipids. Future systematic studies will be required to clearly demonstrate whether and how LMP1 associates with lipid rafts or other preferred lipids. Second, due to the intrinsic flexibility of the LMP1-TRAF complex, we currently provide only the 2D class average results rather than

the high-resolution 3D reconstruction for this sample. Future structural determination of the LMP1-TRAF complex, especially of the full-length proteins, will be necessary to better understand the details of how LMP1 oligomers recruit TRAF proteins.

STAR★METHODS

Detailed methods are provided in the online version of this paper and include the following:

- KEY RESOURCES TABLE
- RESOURCE AVAILABILITY
  - Lead contact
  - Materials availability
  - Data and code availability
- EXPERIMENTAL MODEL AND STUDY PARTICIPANT DETAILS
- METHOD DETAILS
  - Plasmid construction
  - Protein expression and purification
  - Antibody and complex preparation with LMP1
  - Cryo-EM sample preparation and data collection
  - Cryo-EM image processing
  - Model building and analysis
  - Luciferase reporter assays
  - Confocal microscope and TIRF-SIM imaging
  - Flow cytometry
- QUANTIFICATION AND STATISTICAL ANALYSIS

SUPPLEMENTAL INFORMATION

Supplemental information can be found online at https://doi.org/10.1016/j.cell.2024.06.021.

ACKNOWLEDGMENTS

Cryo-EM data collection was carried out at the Center for Biological Imaging, Core Facilities for Protein Science at the Institute of Biophysics, Chinese Academy of Sciences. We thank B. Zhu, T. Niu, L. Chen, X. Huang, G. Ji, F. Sun, and other staff members at the Center for Biological Imaging for their support in data collection. The computation work was performed using high-performance computing resources from the Center for Biological Imaging at the Institute of Biophysics, Chinese Academy of Science. The project was funded by the National Natural Science Foundation of China (32325028, 32130057, 81921005, and 32100757), Basic Research Program Based on Major Scientific Infrastructures-CAS (JZHKYPT-2021-05), Beijing Natural Science Foundation (Z220018), the CAS Project for Young Scientists in Basic Research (YSBR-074), and the Strategic Priority Research Program at the Chinese Academy of Sciences (XDB37030203).

AUTHOR CONTRIBUTIONS

J.H. and Xiaolin Zhang generated most of the data presented here. X.N., Xuyuan Zhang, Y.W., L.H., and X.G. assisted with the experiments. J.H., Xiaolin Zhang, D.L., L.Z., G.G., and P.G. designed the experiments and analyzed the data. J.H., Xiaolin Zhang, L.Z., G.G., and P.G. wrote the manuscript with contributions from all authors. L.Z., G.G., and P.G. initiated the study and directed the research.

DECLARATION OF INTERESTS

The authors declare no competing interests.

Received: December 18, 2023
Revised: May 15, 2024
Accepted: June 18, 2024
Published: July 11, 2024

REFERENCES

1. Young, L.S., Yap, L.F., and Murray, P.G. (2016). Epstein-Barr virus: more than 50 years old and still providing surprises. Nat. Rev. Cancer *16*, 789–802. https://doi.org/10.1038/nrc.2016.92.
2. Lieberman, P.M. (2014). Virology. Epstein-Barr virus turns 50. Science *343*, 1323–1325. https://doi.org/10.1126/science.1252786.
3. Münz, C. (2019). Latency and lytic replication in Epstein-Barr virus-associated oncogenesis. Nat. Rev. Microbiol. *17*, 691–700. https://doi.org/10.1038/s41579-019-0249-7.
4. Elgui de Oliveira, D., Müller-Coan, B.G., and Pagano, J.S. (2016). Viral carcinogenesis beyond malignant transformation: EBV in the progression of human cancers. Trends Microbiol. *24*, 649–664. https://doi.org/10.1016/j.tim.2016.03.008.
5. Wong, Y.D., Meehan, M.T., Burrows, S.R., Doolan, D.L., and Miles, J.J. (2022). Estimating the global burden of Epstein-Barr virus-related cancers. J. Cancer Res. Clin. Oncol. *148*, 31–46. https://doi.org/10.1007/s00432-021-03824-y.
6. Lo, A.K.F., Dawson, C.W., Lung, H.L., Wong, K.L., and Young, L.S. (2021). The role of EBV-encoded LMP1 in the NPC tumor microenvironment: from function to therapy. Front. Oncol. *11*, 640207. https://doi.org/10.3389/fonc.2021.640207.
7. Küppers, R. (2009). The biology of Hodgkin's lymphoma. Nat. Rev. Cancer *9*, 15–27. https://doi.org/10.1038/nrc2542.
8. Thorley-Lawson, D.A., and Allday, M.J. (2008). The curious case of the tumour virus: 50 years of Burkitt's lymphoma. Nat. Rev. Microbiol. *6*, 913–924. https://doi.org/10.1038/nrmicro2015.
9. Zhu, N., Xu, X., Wang, Y., Zeng, M.S., and Yuan, Y. (2021). EBV latent membrane proteins promote hybrid epithelial-mesenchymal and extreme mesenchymal states of nasopharyngeal carcinoma cells for tumorigenicity. PLoS Pathog. *17*, e1009873. https://doi.org/10.1371/journal.ppat.1009873.
10. Awasthi, P., Dwivedi, M., Kumar, D., and Hasan, S. (2023). Insights into intricacies of the latent membrane Protein-1 (LMP-1) in EBV-associated cancers. Life Sci. *313*, 121261. https://doi.org/10.1016/j.lfs.2022.121261.
11. Wilson, J.B., Weinberg, W., Johnson, R., Yuspa, S., and Levine, A.J. (1990). Expression of the BNLF-1 oncogene of Epstein-Barr virus in the skin of transgenic mice induces hyperplasia and aberrant expression of keratin 6. Cell *61*, 1315–1327. https://doi.org/10.1016/0092-8674(90)90695-b.
12. Dawson, C.W., Rickinson, A.B., and Young, L.S. (1990). Epstein-Barr virus latent membrane protein inhibits human epithelial cell differentiation. Nature *344*, 777–780. https://doi.org/10.1038/344777a0.
13. Henderson, S., Rowe, M., Gregory, C., Croom-Carter, D., Wang, F., Longnecker, R., Kieff, E., and Rickinson, A. (1991). Induction of bcl-2 expression by Epstein-Barr virus latent membrane protein 1 protects infected B cells from programmed cell death. Cell *65*, 1107–1115. https://doi.org/10.1016/0092-8674(91)90007-l.
14. Wang, L.W., Jiang, S., and Gewurz, B.E. (2017). Epstein-Barr virus LMP1-mediated oncogenicity. J. Virol. *91*. e01718-16. https://doi.org/10.1128/JVI.01718-16.
15. Raab-Traub, N. (2012). Novel mechanisms of EBV-induced oncogenesis. Curr. Opin. Virol. *2*, 453–458. https://doi.org/10.1016/j.coviro.2012.07.001.
16. Fåhraeus, R., Rymo, L., Rhim, J.S., and Klein, G. (1990). Morphological transformation of human keratinocytes expressing the LMP gene of Epstein-Barr virus. Nature *345*, 447–449. https://doi.org/10.1038/345447a0.
17. Kaye, K.M., Izumi, K.M., and Kieff, E. (1993). Epstein-Barr virus latent membrane protein 1 is essential for B-lymphocyte growth transformation. Proc. Natl. Acad. Sci. USA *90*, 9150–9154. https://doi.org/10.1073/pnas.90.19.9150.

18. Wang, D., Liebowitz, D., and Kieff, E. (1985). An EBV membrane protein expressed in immortalized lymphocytes transforms established rodent cells. Cell *43*, 831–840. https://doi.org/10.1016/0092-8674(85)90256-9.

19. Zhang, B., Kracker, S., Yasuda, T., Casola, S., Vanneman, M., Hömig-Hölzel, C., Wang, Z., Derudder, E., Li, S., Chakraborty, T., et al. (2012). Immune surveillance and therapy of lymphomas driven by Epstein-Barr virus protein LMP1 in a mouse model. Cell *148*, 739–751. https://doi.org/10.1016/j.cell.2011.12.031.

20. Middeldorp, J.M., and Pegtel, D.M. (2008). Multiple roles of LMP1 in Epstein-Barr virus induced immune escape. Semin. Cancer Biol. *18*, 388–396. https://doi.org/10.1016/j.semcancer.2008.10.004.

21. Dukers, D.F., Meij, P., Vervoort, M.B., Vos, W., Scheper, R.J., Meijer, C.J., Bloemena, E., and Middeldorp, J.M. (2000). Direct immunosuppressive effects of EBV-encoded latent membrane protein 1. J. Immunol. *165*, 663–670. https://doi.org/10.4049/jimmunol.165.2.663.

22. Pratt, Z.L., Zhang, J., and Sugden, B. (2012). The latent membrane protein 1 (LMP1) oncogene of Epstein-Barr virus can simultaneously induce and inhibit apoptosis in B cells. J. Virol. *86*, 4380–4393. https://doi.org/10.1128/JVI.06966-11.

23. Choi, I.K., Wang, Z., Ke, Q., Hong, M., Qian, Y., Zhao, X., Liu, Y., Kim, H.J., Ritz, J., Cantor, H., et al. (2018). Signaling by the Epstein-Barr virus LMP1 protein induces potent cytotoxic CD4(+) and CD8(+) T cell responses. Proc. Natl. Acad. Sci. USA *115*, E686–E695. https://doi.org/10.1073/pnas.1713607115.

24. Jiang, S., Zhou, H., Liang, J., Gerdt, C., Wang, C., Ke, L., Schmidt, S.C.S., Narita, Y., Ma, Y., Wang, S., et al. (2017). The Epstein-Barr virus Regulome in lymphoblastoid cells. Cell Host Microbe *22*, 561–573.e4. https://doi.org/10.1016/j.chom.2017.09.001.

25. Choi, I.K., Wang, Z., Ke, Q., Hong, M., Paul, D.W., Jr., Fernandes, S.M., Hu, Z., Stevens, J., Guleria, I., Kim, H.J., et al. (2021). Mechanism of EBV inducing anti-tumour immunity and its therapeutic use. Nature *590*, 157–162. https://doi.org/10.1038/s41586-020-03075-w.

26. Kang, Y., He, W., Ren, C., Qiao, J., Guo, Q., Hu, J., Xu, H., Jiang, X., and Wang, L. (2020). Advances in targeted therapy mainly based on signal pathways for nasopharyngeal carcinoma. Signal Transduct. Target. Ther. *5*, 245. https://doi.org/10.1038/s41392-020-00340-2.

27. Uchida, J., Yasui, T., Takaoka-Shichijo, Y., Muraoka, M., Kulwichit, W., Raab-Traub, N., and Kikutani, H. (1999). Mimicry of CD40 signals by Epstein-Barr virus LMP1 in B lymphocyte responses. Science *286*, 300–303. https://doi.org/10.1126/science.286.5438.300.

28. Gires, O., Zimber-Strobl, U., Gonnella, R., Ueffing, M., Marschall, G., Zeidler, R., Pich, D., and Hammerschmidt, W. (1997). Latent membrane protein 1 of Epstein-Barr virus mimics a constitutively active receptor molecule. EMBO J. *16*, 6131–6140. https://doi.org/10.1093/emboj/16.20.6131.

29. Kaykas, A., Worringer, K., and Sugden, B. (2001). CD40 and LMP-1 both signal from lipid rafts but LMP-1 assembles a distinct, more efficient signaling complex. EMBO J. *20*, 2641–2654. https://doi.org/10.1093/emboj/20.11.2641.

30. Mosialos, G., Birkenbach, M., Yalamanchili, R., VanArsdale, T., Ware, C., and Kieff, E. (1995). The Epstein-Barr virus transforming protein LMP1 engages signaling proteins for the tumor necrosis factor receptor family. Cell *80*, 389–399. https://doi.org/10.1016/0092-8674(95)90489-1.

31. Bentz, G.L., Whitehurst, C.B., and Pagano, J.S. (2011). Epstein-Barr virus latent membrane protein 1 (LMP1) C-terminal-activating region 3 contributes to LMP1-mediated cellular migration via its interaction with Ubc9. J. Virol. *85*, 10144–10153. https://doi.org/10.1128/JVI.05035-11.

32. Eliopoulos, A.G., and Young, L.S. (2001). LMP1 structure and signal transduction. Semin. Cancer Biol. *11*, 435–444. https://doi.org/10.1006/scbi.2001.0410.

33. Coffin, W.F., Geiger, T.R., and Martin, J.M. (2003). Transmembrane domains 1 and 2 of the latent membrane protein 1 of Epstein-Barr virus contain a lipid raft targeting signal and play a critical role in cytostasis. J. Virol. *77*, 3749–3758. https://doi.org/10.1128/Jvi.77.6.3749-3758.2003.

34. Yasui, T., Luftig, M., Soni, V., and Kieff, E. (2004). Latent infection membrane protein transmembrane FWLY is critical for intermolecular interaction, raft localization, and signaling. Proc. Natl. Acad. Sci. USA *101*, 278–283. https://doi.org/10.1073/pnas.2237224100.

35. Soni, V., Yasui, T., Cahir-McFarland, E., and Kieff, E. (2006). LMP1 transmembrane domain 1 and 2 (TM1-2) FWLY mediates intermolecular interactions with TM3-6 to activate NF-κB. J. Virol. *80*, 10787–10793. https://doi.org/10.1128/JVI.01214-06.

36. Lee, J., and Sugden, B. (2007). A membrane leucine heptad contributes to trafficking, signaling, and transformation by latent membrane protein 1. J. Virol. *81*, 9121–9130. https://doi.org/10.1128/JVI.00136-07.

37. Erickson, K.D., and Martin, J.M. (2000). The late lytic LMP-1 protein of Epstein-Barr virus can negatively regulate LMP-1 signaling. J. Virol. *74*, 1057–1060. https://doi.org/10.1128/Jvi.74.2.1057-1060.2000.

38. Wang, D., Liebowitz, D., and Kieff, E. (1988). The truncated form of the Epstein-Barr virus latent-infection membrane-protein expressed in virus-replication does not transform rodent fibroblasts. J. Virol. *62*, 2337–2346. https://doi.org/10.1128/JVI.62.7.2337-2346.1988.

39. Kaykas, A., Worringer, K., and Sugden, B. (2002). LMP-1's transmembrane domains encode multiple functions required for LMP-1's efficient signaling. J. Virol. *76*, 11551–11560. https://doi.org/10.1128/jvi.76.22.11551-11560.2002.

40. Holm, L. (2020). Using Dali for protein structure comparison. Methods Mol. Biol. *2112*, 29–42. https://doi.org/10.1007/978-1-0716-0270-6_3.

41. Jumper, J., Evans, R., Pritzel, A., Green, T., Figurnov, M., Ronneberger, O., Tunyasuvunakool, K., Bates, R., Žídek, A., Potapenko, A., et al. (2021). Highly accurate protein structure prediction with AlphaFold. Nature *596*, 583–589. https://doi.org/10.1038/s41586-021-03819-2.

42. Verweij, F.J., van Eijndhoven, M.A.J., Hopmans, E.S., Vendrig, T., Wurdinger, T., Cahir-McFarland, E., Kieff, E., Geerts, D., van der Kant, R., Neefjes, J., et al. (2011). LMP1 association with CD63 in endosomes and secretion via exosomes limits constitutive NF-kappaB activation. EMBO J. *30*, 2115–2129. https://doi.org/10.1038/emboj.2011.123.

43. Wu, S., Xie, P., Welsh, K., Li, C., Ni, C.Z., Zhu, X., Reed, J.C., Satterthwait, A.C., Bishop, G.A., and Ely, K.R. (2005). LMP1 protein from the Epstein-Barr virus is a structural CD40 decoy in B lymphocytes for binding to TRAF3. J. Biol. Chem. *280*, 33620–33626. https://doi.org/10.1074/jbc.M502511200.

44. Baxendale, A.J., Dawson, C.W., Stewart, S.E., Mudaliar, V., Reynolds, G., Gordon, J., Murray, P.G., Young, L.S., and Eliopoulos, A.G. (2005). Constitutive activation of the CD40 pathway promotes cell transformation and neoplastic growth. Oncogene *24*, 7913–7923. https://doi.org/10.1038/sj.onc.1208929.

45. Mitchell, T., and Sugden, B. (1995). Stimulation of NF-kappa B-mediated transcription by mutant derivatives of the latent membrane protein of Epstein-Barr virus. J. Virol. *69*, 2968–2976. https://doi.org/10.1128/JVI.69.5.2968-2976.1995.

46. Dirmeier, U., Neuhierl, B., Kilger, E., Reisbach, G., Sandberg, M.L., and Hammerschmidt, W. (2003). Latent membrane protein 1 is critical for efficient growth transformation of human B cells by Epstein-Barr virus. Cancer Res. *63*, 2982–2989.

47. Pandya, J., and Walling, D.M. (2004). Epstein-Barr virus latent membrane protein 1 (LMP-1) half-life in epithelial cells is down-regulated by lytic LMP-1. J. Virol. *78*, 8404–8410. https://doi.org/10.1128/JVI.78.15.8404-8410.2004.

48. Pandya, J., and Walling, D.M. (2006). Oncogenic activity of Epstein-Barr virus latent membrane protein 1 (LMP-1) is down-regulated by lytic LMP-1. J. Virol. *80*, 8038–8046. https://doi.org/10.1128/JVI.00180-06.

49. Smith, C., Wakisaka, N., Crough, T., Peet, J., Yoshizaki, T., Beagley, L., and Khanna, R. (2009). Discerning regulation of cis- and trans-presentation of CD8+ T-cell epitopes by EBV-encoded oncogene LMP-1 through self-aggregation. Blood *113*, 6148–6152. https://doi.org/10.1182/blood-2009-02-203687.

50. Taylor, G.S., Long, H.M., Brooks, J.M., Rickinson, A.B., and Hislop, A.D. (2015). The immunology of Epstein-Barr virus Induced Disease. Annu. Rev. Immunol. *33*, 787–821. https://doi.org/10.1146/annurev-immunol-032414-112326.

51. Punjani, A., Rubinstein, J.L., Fleet, D.J., and Brubaker, M.A. (2017). cryoSPARC: algorithms for rapid unsupervised cryo-EM structure determination. Nat. Methods *14*, 290–296. https://doi.org/10.1038/nmeth.4169.

52. Adams, P.D., Afonine, P.V., Bunkóczi, G., Chen, V.B., Echols, N., Headd, J.J., Hung, L.W., Jain, S., Kapral, G.J., Grosse Kunstleve, R.W., et al. (2011). The Phenix software for automated determination of macromolecular structures. Methods *55*, 94–106. https://doi.org/10.1016/j.ymeth.2011.07.005.

53. Pettersen, E.F., Goddard, T.D., Huang, C.C., Couch, G.S., Greenblatt, D.M., Meng, E.C., and Ferrin, T.E. (2004). UCSF Chimera–a visualization system for exploratory research and analysis. J. Comput. Chem. *25*, 1605–1612. https://doi.org/10.1002/jcc.20084.

54. Goddard, T.D., Huang, C.C., Meng, E.C., Pettersen, E.F., Couch, G.S., Morris, J.H., and Ferrin, T.E. (2018). UCSF ChimeraX: meeting modern challenges in visualization and analysis. Protein Sci. *27*, 14–25. https://doi.org/10.1002/pro.3235.

55. Emsley, P., and Cowtan, K. (2004). Coot: model-building tools for molecular graphics. Acta Crystallogr. D Biol. Crystallogr. *60*, 2126–2132. https://doi.org/10.1107/S0907444904019158.

56. Zheng, S.Q., Palovcak, E., Armache, J.P., Verba, K.A., Cheng, Y., and Agard, D.A. (2017). MotionCor2: anisotropic correction of beam-induced motion for improved cryo-electron microscopy. Nat. Methods *14*, 331–332. https://doi.org/10.1038/nmeth.4193.

57. Schindelin, J., Arganda-Carreras, I., Frise, E., Kaynig, V., Longair, M., Pietzsch, T., Preibisch, S., Rueden, C., Saalfeld, S., Schmid, B., et al. (2012). Fiji: an open-source platform for biological-image analysis. Nat. Methods *9*, 676–682. https://doi.org/10.1038/nmeth.2019.

STAR★METHODS

KEY RESOURCES TABLE

REAGENT or RESOURCE	SOURCE	IDENTIFIER
Antibodies		
4E9	This paper	N/A
Anti-EBV Latent Membrane Protein 1 antibody	abcam	Cat# ab78113; RRID: AB_1566182
ACTB Rabbit mAb	Abclonal	Cat# AC038; RRID: AB_2863784
Anti-Mouse IgG (H+L) antibody, HRP Conjugate	Promega	Cat# W4021; RRID: AB_430834
Peroxidase-Conjugated Goat anti-Rabbit IgG(H+L)	ZSGB-Bio	Cat# ZB-2301; RRID: AB_2747412
PE Goat anti-mouse IgG	Biolegend	Cat# 405307; RRID: AB_315010
Goat Anti-Mouse IgG (whole molecule) Polyclonal Antibody, TRITC Conjugated	Sigma-Aldrich	Cat# T5393; RRID: AB_261699
Fc Receptor Binding Inhibitor Polyclonal Antibody	Thermo Fisher Scientific	Cat# 14-9161-73; RRID: AB_468582
Purified Mouse IgG2b, κ Isotype Ctrl Antibody	Biolegend	Cat# 400301; RRID: AB_326481
Bacterial and virus strains		
E. c. BL21 Chemically Competent Cell	Tsingke	Cat#TSC-E01
E. c. Top10 Chemically Competent Cell	TransGen	Cat#CD101-01
Chemicals, peptides, and recombinant proteins		
n-dodecyl-β-d-maltopyranoside (DDM)	Anatrace	Cat# D310
n-Nonyl-β-D-glucopyranoside (β-NG)	Anatrace	Cat# N324
Ni^{2+}-nitrilotriacetate affinity resin (Ni-NTA)	QIAGEN	Cat# 30250
Superdex 200 Increase 10/300 GL column	GE Healthcare	Cat# 28-9909-44
Lipofectamine 2000	Thermo Fisher Scientific	Cat# 11668019
Xpregen	Beijing Yu-Feng Biotechnology	Cat# ND01
Doxycycline	Sigma-Aldrich	Cat# D9891
Puromycin	Sigma-Aldrich	Cat# P9620
TPA (12-O-Tetradecanoylphorbol-13-Acetate)	Sigma-Aldrich	Cat# P8139
Antifade Mounting Medium with DAPI	Beyotime Biotechnology	Cat# P0131
Permeabilization buffer(10X)	Thermo Fisher Scientific	Cat# 00-8333-56
4% Paraformaldehyde Fix Solution	Solarbio	Cat# P1110
Normal human serum	Beijing CellChip Biotechnology	Cat# 070028-H1
Normal sheep serum	Solarbio	Cat# SL039
Critical commercial assays		
Pierce™ Fab Preparation Kit	Thermo Fisher Scientific	Cat#44985
Dual-Luciferase® Reporter Assay System	Promega	Cat# E1910
SF Cell Line 4D-Nucleofector™ X Kit	Lonza	Cat# V4XC-2024
Deposited data		
LMP1 dimer coordinates	This paper	PDB: 8XH6
LMP1 dimer EM map	This paper	EMDB: EMD-38342
LMP1 oligomer coordinates	This paper	PDB: 8XH7
LMP1 oligomer EM map	This paper	EMDB: EMD-38343

(*Continued on next page*)

Continued

REAGENT or RESOURCE	SOURCE	IDENTIFIER
Experimental models: Cell lines		
HEK293	ATCC	CRL-1573
293T	ATCC	CRL-11268
HeLa	ATCC	CCL-2
HeLa-EGFP-LMP1	This paper	N/A
Daudi	ATCC	CCL-213
B95-8	ATCC	CRL-1612
Oligonucleotides		
See Table S3 for the sequence information of primers	Tsingke	N/A
Recombinant DNA		
Full-length LMP1	This paper	N/A
LMP1(25-186)	This paper	N/A
TRAF3(313-504)	This paper	N/A
See Table S2 for the mutants of LMP1	This paper	N/A
Software and algorithms		
CryoSPARC v4.2.1	Punjani et al.[51]	https://cryosparc.com
PHENIX 1.17	Adams et al.[52]	http://www.phenix-online.org/
UCSF Chimera	Pettersen et al.[53]	https://www.cgl.ucsf.edu/chimera/
UCSF Chimera X	Goddard et al.[54]	https://www.cgl.ucsf.edu/chimerax/
Coot v0.8.3	Emsley and Cowtan[55]	https://www2.mrc-lmb.cam.ac.uk/personal/pemsley/coot/
Graphpad Prism	GraphPad software	https://www.graphpad.com/
Pymol	Schrodinger	https://pymol.org/2/
MotionCor2	Zheng et al.[56]	https://emcore.ucsf.edu/ucsf-software
ImageJ	Schindelin et al.[57]	https://fiji.sc
FlowJo	FlowJo software	https://www.flowjo.com/solutions/flowjo

RESOURCE AVAILABILITY

Lead contact

Further information and requests for resources and reagents should be directed to and will be fulfilled by the lead contact, Pu Gao (gaopu@ibp.ac.cn).

Materials availability

The study did not generate new unique materials or reagents.

Data and code availability

- The atomic coordinates have been deposited at the Protein Data Bank under accession numbers 8XH6 (LMP1 dimer) and 8XH7 (LMP1 oligomer). The cryo-EM density maps have been deposited at the Electron Microscopy Data Bank under accession numbers EMD-38342 (LMP1 dimer) and EMD-38343 (LMP1 oligomer).
- This paper does not report original code.
- Any additional information required to reanalyze the data reported in this paper is available from the lead contact upon request.

EXPERIMENTAL MODEL AND STUDY PARTICIPANT DETAILS

E. coli Top10 Chemically Competent Cells were used for molecular cloning. *E. coli* BL21(DE3) Chemically Competent Cells were used for protein expression. All *E. coli* cells were cultured in LB medium at 37°C.

HEK293 (ATCC CRL-1573), HeLa (ATCC CCL-2), 293T (ATCC CRL-11268) and HeLa-EGFP-LMP1 (this study) cells were maintained in DMEM supplemented with 10% FBS (sigma) at 37°C, 5% CO_2.

Daudi (ATCC CCL-213), B95-8 (ATCC CRL-1612) cells were cultured at 37°C and 5% CO_2 in RPMI 1640 supplemented with 10% heat-inactivated fetal bovine serum, penicillin, and streptomycin.

To generate HeLa cells expressing GFP-LMP1^{fl} in a doxycycline-inducible manner, pTripZ-EGFP-LMP1 was packaged into a VSV_G pseudotyped lentivector in 293T cells to transduce HeLa cells, followed by selection in puromycin-containing medium. Doxycycline-inducible expression of GFP-LMP1^{fl} was detected by flow cytometry and western blotting.

METHOD DETAILS

Plasmid construction

The nucleotide sequences of LMP1 from Human gammaherpesvirus 4 (NCBI protein accession AAQ16193.1) and TRAF3 from Homo sapiens (NCBI protein accession NP_003291.2) were synthesized and codon-optimized for expression in *E. coli*. The full-length LMP1 gene (LMP1^{fl}) and the LMP1 transmembrane region (aa 25–186) were cloned into the modified pCDFDuet vector (Novagen) with a cleavable N-terminal BRIL tag linearized by BamHI and XhoI. The TRAF3 gene (aa 313–504) was cloned into the modified pRSF-Duet-1 vector (Novagen) with a cleavable N-terminal His6-SUMO tag linearized by BamHI and XhoI.

pTK-LMP1 or indicated mutations express either LMP1^{fl} or site-directed mutations (dimer-mut, dimer-mut1, dimer-mut2, dimer-mut3, dimer-mut4, dimer-mut5, dimer-mut1+2, dimer-mut1+3, dimer-mut2+3, oligomer-mut, oligomer-mut1, oligomer-mut2, oligomer-mut3, oligomer-mut4, oligomer-mut5, oligomer-mut1+2, oligomer-mut1+3, oligomer-mut2+3), respectively, under the transcription control of the TK promoter. To construct pTK-LMP1, the renilla luciferase coding sequence in the pRL-TK vector (Promega, E2241) was replaced with the LMP1 coding sequence. pLenti-EF1α-EGFP-LMP1 is a third generation lentiviral plasmid for expression of N-terminal EGFP fused LMP1^{fl} under the transcriptional control of the EF1α promoter. N-terminal GFP fused LMP1 mutations were also inserted into the pLenti-EF1α vector for transduced into HeLa cells. The EGFP-LMP1 coding sequence was cloned into the lentivector pTripZ (Horizon) to express N-terminal EGFP fused LMP1^{fl} in a doxycycline-inducible manner. The AP-1 reporter, AP-1-luc (Yeasen Biotechnology, 11535ES03), contains the firefly luciferase gene under the control of multimerized AP-1 responsive elements located upstream of a minimal promoter. The NF-κB-luc reporter was a generous gift from Dr. Hongbing Shu (Wuhan University, China). Plasmid transfection was performed using Xpregen following the manufacturer's instructions (Beijing Yu-Feng Biotechnology).

All primers used in this report are listed in Table S3. All constructs were confirmed by DNA sequencing.

Protein expression and purification

Vector expression was carried out in *E. coli* BL21(DE3) cells that were grown aerobically at 37°C in lysogeny broth (LB) medium containing 50 μg mL^{-1} streptomycin or kanamycin. His6-SUMO-tagged TRAF3 and His6-BRIL-tagged (LMP1^{fl} and LMP1$^{26–187}$) constructs were transfected into *E. coli* BL21(DE3) cells. The cells were cultured at 37°C until OD_{600} reached 0.6–0.8. The temperature was then shifted to 25°C and the cells were induced by adding 0.5 mM isopropyl-β-d-1-thiogalactopyranoside (IPTG) for 16 h with constant shaking. Cells were collected and lysed by sonication in lysis buffer (25 mM Tris-HCl, pH 7.5, 150 mM NaCl, 20 mM imidazole, and 1 mM PMSF). For LMP1 purification, the suspension was further supplemented with 1% (w/v) n-dodecyl-β-d-maltopyranoside (DDM, Anatrace). After incubation at 4°C overnight, the mixture was centrifuged at 35,000 × g for 30 min, and the supernatant was applied to Ni affinity resin. The resin was rinsed with wash buffer containing 25 mM Tris-HCl, pH 7.5, 150 mM NaCl, 50 mM imidazole, and 0.03% DDM, then, eluted with wash buffer plus 500 mM imidazole. The His6-BRIL tag was cleaved by adding TEV protease and reloading the protein sample onto the Ni column to remove the His6-BRIL tag and the TEV protease. The flow-through was concentrated using a 100-kDa cut-off Amicon (Millipore) filter and further purified through size-exclusion chromatography on a Superdex 200 Increase 10/300 GL column (GE Healthcare) that was preequilibrated in buffer containing 25 mM Tris-HCl, pH 7.5, 150 mM NaCl, and 0.03% DDM (or 0.4% β-NG). The peak fractions were pooled and concentrated to about 10 mg mL^{-1} followed by storage at –80°C for later use. For soluble TRAF3, the cell lysates were centrifuged at 25,000 × g for 30 min at 4°C and the supernatant was purified using Ni-NTA beads. The His6-SUMO tag from TRAF3 was removed by overnight ULP1 protease digestion and the sample was reloaded onto the Ni column to remove the His6-SUMO tag and the ULP1 protease. The flow through was concentrated using a 10 kDa cut-off Amicon (Millipore) filter and further purified through size-exclusion chromatography on a Superdex 200 Increase 10/300 GL column (GE Healthcare) that was preequilibrated in buffer containing 25 mM Tris-HCl, pH 7.5 and 150 mM NaCl. The peak fractions were pooled and concentrated to about 10 mg mL^{-1} followed by storage at –80°C for later use. For the LMP1^{fl}-TRAF3 complex, LMP1^{fl} and TRAF3 were mixed at a molar ratio of 1:1.2 and incubated at 4°C with constant rotation for 20 min. Subsequently, the sample was loaded onto the Superdex 200 10/300 GL column and eluted with 25 mM Tris-HCl, pH 7.5, 150 mM NaCl, and 0.4% β-NG. Peak fractions containing pure proteins were pooled and concentrated for cryo-EM.

Antibody and complex preparation with LMP1

Monoclonal antibodies against LMP1 (clone 4E9) for cryo-EM were raised by immunizing mice with purified LMP1 dimer sample (residues 25-186; same as the construct for cryo-EM) and screening by hybridoma technology. 293T cells transfected with the full-length LMP1 expression plasmid were used to screen the LMP1-binding antibody-secreting clones by flow cytometry. The Fab fragment used in cryo-EM reconstructions was generated using the Pierce Fab Preparation Kit (Thermo Fisher Scientific). For the LMP1-Fab complex, LMP1 and Fab were mixed at a molar ratio of 1:1.2 and incubated at 4°C with constant rotation for 20 min. The sample

was then loaded onto a Superdex 200 10/300 GL and eluted with 25 mM Tris-HCl, pH 7.5, 50 mM NaCl, and 0.03% DDM for dimer sample, or 0.4% β-NG for filament sample. Peak fractions containing pure proteins were pooled and concentrated for cryo-EM.

Cryo-EM sample preparation and data collection

A total of 3.5 μl of purified LMP1-Fab (dimer) and LMP1-Fab (filament) complexes at a concentration of 15 mg mL^{-1} were applied to a glow-discharged Quantifoil grid (R 1.2/1.3 300 mesh, Cu, Electron Microscopy Sciences), blotted for 3 s in 100% humidity at 4°C and plunged into liquid ethane using a Vitrobot Mark IV (Thermo Fisher Scientific). Data collection of the cryo-EM datasets of LMP1-Fab (dimer) and LMP1-Fab (filament) were performed on a 300 kV titan Krios electron microscope (FEI) equipped with K2 Summit camera (Gatan), and a GIF Quantum energy filter operated with a slit width of 20 eV. All cryo-EM super-resolution micrographs were collected automatically using the Serial-EM package, yielding an image stack with a pixel size of 1.04 Å. All the images were recorded at a defocus range of –1.2 mm to –1.8 mm, with a total electron dose of 60 electrons per $Å^2$ over 32 movie frames during a total exposure time of 4 s. Images were recorded by beam-image shift data collection methods. Each movie stack was motion-corrected by MotionCor2.[56] The dose-weighted micrographs were kept for further image processing using CryoSPARC v4.3.0.[51]

Cryo-EM image processing

After data collection, the exact defocus value and contrast transfer function (CTF) of each micrograph were estimated using CryoSPARC's patch CTF estimation tool. Particles were automatically picked using Blob picking and Templet picking. For the data of LMP1-Fab (dimer), a total of 5,055,975 particles were auto-picked from 8,529 micrographs. After 2D and 3D classification, 507,458 particles with good features were kept for further data processing (Figures S3A–S3C). Two further rounds of 3D classification were performed with a model created in CryoSPARC and low-pass filtered to 60 Å as a reference map, generating the best class containing 348,350 particles for further non-uniform refinement with C1 symmetry. After Bayesian polishing and local 3D refinement, an improved map for the whole complex yielded a resolution of 3.5 Å, whose resolution was estimated based on the gold-standard Fourier shell correlation (FSC) with 0.143 criterion. For the data of LMP1-Fab (filament), a total of 10,157,152 particles were auto-picked from 14,174 micrographs. After 2D and 3D classification, 956,722 particles with good features were kept for further data processing (Figures S3D–S3F). After removing the duplicate particles, three rounds of 3D classification were performed with a model created in CryoSPARC and low-pass filtered to 60 Å as a reference map. A total of 387,083 particles were used for further non-uniform refinement with C2 symmetry resulting in a 3.5 Å map, whose resolution was estimated based on the gold-standard Fourier shell correlation (FSC) with 0.143 criterion.

Model building and analysis

The structure of LMP1 predicted by AlphaFold2 (Figure S6),[41] as the initial model, did not fit into the cryo-EM maps using UCSF Chimera.[53] Thus, we rebuilt the Initial structure model based on the cryo-EM density map. The resulting model was then manually rebuilt in COOT.[55] PHENIX was used to refine the model against the cryo-EM density in real space and to ensure proper geometry. The model stereochemistry was evaluated using the comprehensive validation (Cryo-EM) utility in PHENIX.[52] Structural figures were generated using PyMOL (The PyMOL Molecular Graphics System, Version 2.0 Schrödinger, LLC.) and ChimeraX.[54] Model versus map FSC curves were calculated using Phenix to obtain an estimate of the final resolution for the models. Pairwise structure comparison was performed on the Dali server.[40]

Luciferase reporter assays

HEK293 cells were transfected with NF-κB-luc or AP-1-luc reporter, pRL-TK vector, together with pTK-LMP1 or indicated mutations for 24 h. The cells were then lysed in passive lysis buffer (Promega). Firefly and Renilla luciferase activities were measured using the dual-luciferase reporter assay system (Promega). Firefly luciferase activity was normalized with the Renilla luciferase activity. NF-κB or AP-1 activation was calculated as fold induction compared with pTK empty vector transfected controls.

To analyze the effects of representative LMP1 mutants in established lymphoid cell lines, NF-κB-luc, pRL-TK vector, together with pTK-LMP1 or indicated mutations were electroporated into Daudi cells using the SF Cell Line 4D-Nucleofector™ X Kit (Lonza V4XC-2024) and program CA139 in the Lonza 4D-Nucleofector X-Unit platform, followed by luciferase assays and immunoblotting of LMP1 and β-actin.

For the luciferase assay in doxycycline-inducible HeLa-EGFP-LMP1 cells, NF-κB-luc reporter and pRL-TK vector were transfected into cells using lipofectamine 2000 (Thermo Fisher) following the manufacturer's instruction. At 8 h post-transfection, cells in 60 mm dishes were reseeded into nine wells of 12-well plates and cultured overnight. Cells were then mock-treated or treated with different concentrations of doxycycline for 6 hours to induce gradient GFP-$LMP1^{fl}$ expression, followed by luciferase assays.

Confocal microscope and TIRF-SIM imaging

HeLa cells were seeded onto glass bottom dishes (Cellvis) overnight and cells were transduced with pLenti-EF1α-EGFP-LMP1 or indicated mutations. At 24 hours post transduction, cells were fixed with 4% paraformaldehyde and washed with PBS. Samples were then photographed using a Laser Confocal Microscope (Olympus FV3000RS). For super-resolution imaging of LMP1 and mutants, live cells were placed into the imaging chamber of Multi-SIM (Beijing NanoInsights-tech Co., Ltd) at 37°C with controlled humidity and CO_2, after 24 h post-transduction. The specimens were then imaged in the TIRF-SIM mode. To measure the filament

formation and filament length distribution of LMP1 at different expression levels, HeLa-EGFP-LMP1 cells seeded onto glass bottom dishes (Cellvis) were mock-treated or treated with different concentrations of doxycycline for 6 h, followed by SIM imaging.

For fluorescent staining assay in EBV-infected cells, B95-8 cells were induced in growth medium by adding 12-O-tetradecanoylphorbol-13-acetate (TPA; 20 ng/ml; Sigma) for 3 days. Cells were then fixed with 4% paraformaldehyde, washed with PBS, and permeabilized with 0.2% Triton X-100. After blocking in staining buffer (10% human serum (Beijing CellChip Biotechnology), 10% normal sheep serum (Solarbio) and 10 μg/ml Fc receptor blocker (Thermo Fisher Scientific, 14-9161-73) in PBS), samples were stained with LMP1 Ab-4E9 (10μg/ml) or Ab-CTD (3μg/ml, abcam, ab78113) and TRITC-conjugated secondary antibody (Sigma, T5393). Subsequently, the samples were washed with PBS, cytospun onto microscope glass slides, and mounted with Antifade Mounting Medium with DAPI (Beyotime). The subcellular localization of the stained proteins was photographed using a Laser Confocal Microscope (OLYMPUS FV3000RS). Images were rendered and cropped for visualization using Fiji ImageJ.[57] Plotting and statistical analysis were performed using Prism (GraphPad).

Flow cytometry

B95-8 cells, with or without induction by TPA, were fixed, permeabilized (eBioscience) and then stained with a corresponding panel of LMP1-specific or isotype control antibodies. To inhibit the non-specific binding of LMP1 monoclonal antibodies, samples were incubated for 30 min on ice with 10% normal human serum (Beijing CellChip Biotechnology), 10% normal sheep serum (Solarbio) and the Fc Receptor Binding Inhibitor (Thermo Fisher Scientific). Without washing, cells were stained with LMP1 Ab-4E9, Ab-CTD (abcam, ab78113) or isotype control (BioLegend). Cells were then washed with PBS and incubated with PE Goat anti-mouse IgG Antibody (BioLegend). An Attune NxT Flow Cytometer (Thermo Fisher Scientific) with Attune Cytometric software was used for data acquisition; FlowJo software was used for post-acquisition analysis.

QUANTIFICATION AND STATISTICAL ANALYSIS

Statistical analyses were performed using Graphpad Prism software and data were presented as mean ± SD calculated from three independent experiments. All reported resolutions in cryo-EM studies are based upon the 0.143 Fourier Shell Correlation criterion.

Supplemental figures

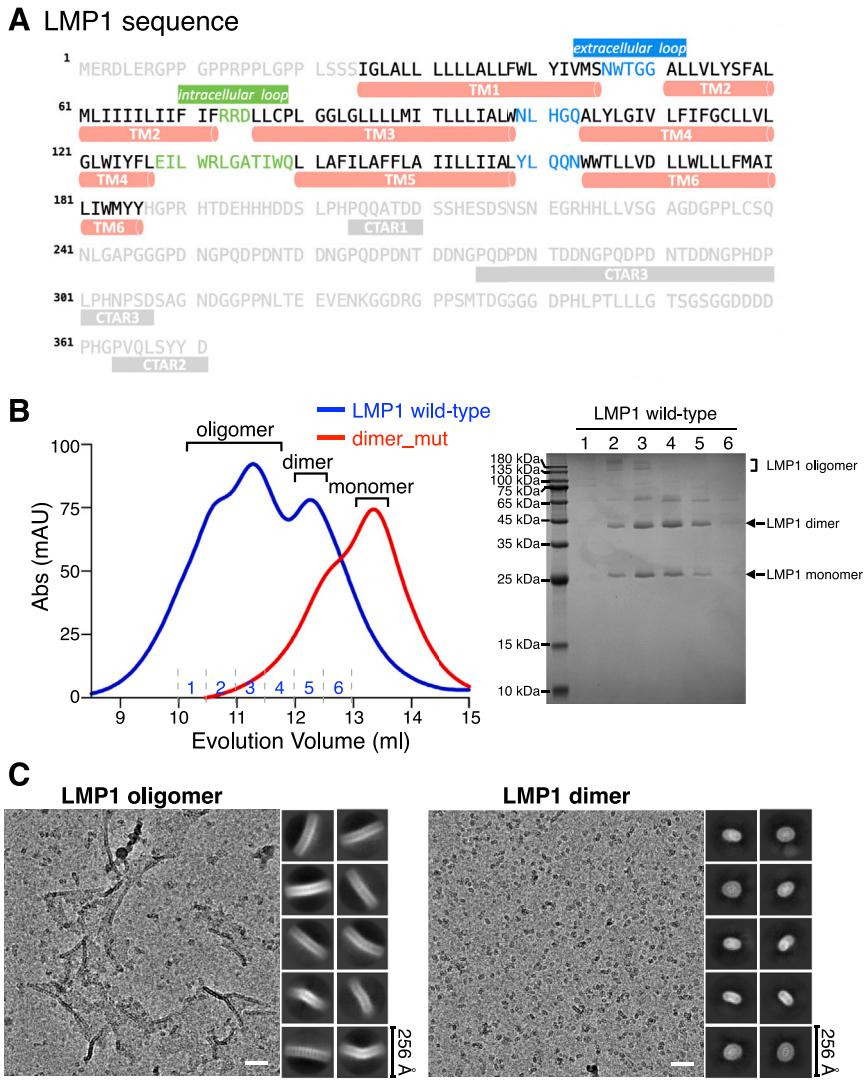

Figure S1. Purification and characterization of EBV LMP1, related to Figure 1

(A) Sequence analysis of EBV LMP1. Red barrels represent transmembrane helices. The intracellular (73–75; 128–139) and extracellular (56–60; 98–103; 158–163) loops are highlighted in green and blue, respectively. The unstructured N- and C-terminal tails (1–24 and 187–371) are shown in gray. LMP1 contains three signaling domains, the C-terminal activation regions 1, 2, and 3 (CTAR1, CTAR2, and CTAR3).

(B) Size-exclusion chromatography of wild-type LMP1 and LMP1 dimer_mut on a Superdex 200 Increase 10/300 GL column. SEC profile and SDS-PAGE analysis of the LMP1 showing the presence of both dimeric and higher-order oligomeric LMP1 fractions.

(C) Representative micrographs and cryo-EM 2D class averages of LMP1 oligomer (left) and LMP1 dimer (right). Scale bars, 50 nm.

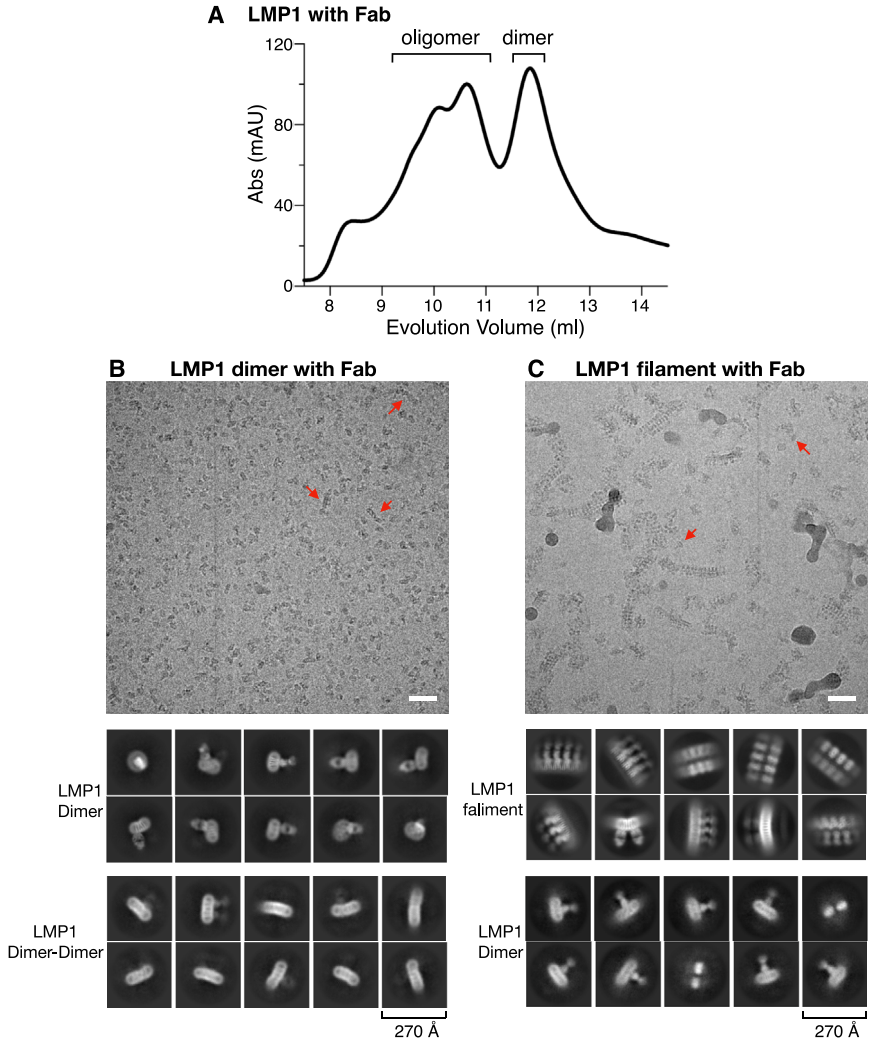

Figure S2. LMP1 transitions between dimer and oligomer conformations, related to Figure 1

(A) Size-exclusion chromatography profile of the LMP1-Fab complex on a Superdex 200 Increase 10/300 GL column showing the presence of both dimeric and higher-order oligomeric LMP1-Fab fractions.

(B and C) Representative micrographs and cryo-EM 2D class averages of LMP1-Fab dimer (B) and LMP1-Fab oligomer (C) show the presence of both dimeric and oligomeric forms in each sample. The red arrows in (B) indicate the presence of some LMP1 oligomer particles in the LMP1 dimer grid; The red arrows in (C) indicate the presence of some LMP1 dimer particles in the LMP1 oligomer grid. Scale bars, 50 nm.

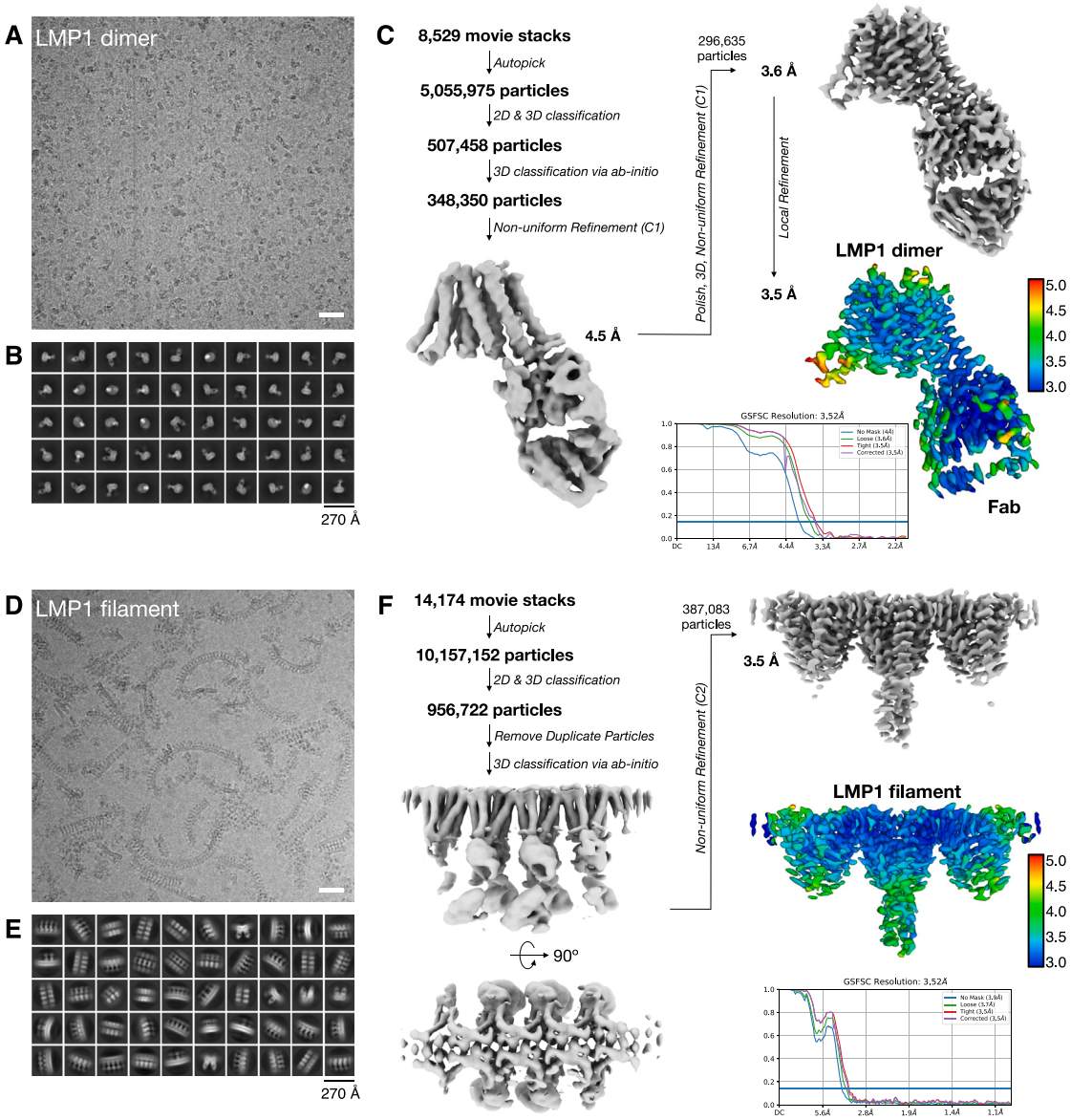

Figure S3. Flow chart of cryo-EM image processing for LMP1 dimer and LMP1 oligomer, related to Figures 1, 2, and 3

(A) Representative micrograph for LMP1 dimer. Scale bars, 50 nm.

(B) Representative 2D classes of LMP1 dimer.

(C) Image processing procedure and final reconstructions of LMP1 dimer. Gold-standard Fourier shell correlation (FSC) curves of the final 3D reconstructions of LMP1 dimer.

(D) Representative micrograph for LMP1 oligomer. Scale bars, 50 nm.

(E) Representative 2D classes of LMP1 oligomer.

(F) Image processing procedure and final reconstructions of LMP1 oligomer. Gold-standard FSC curves of the final 3D reconstructions of LMP1 oligomer.

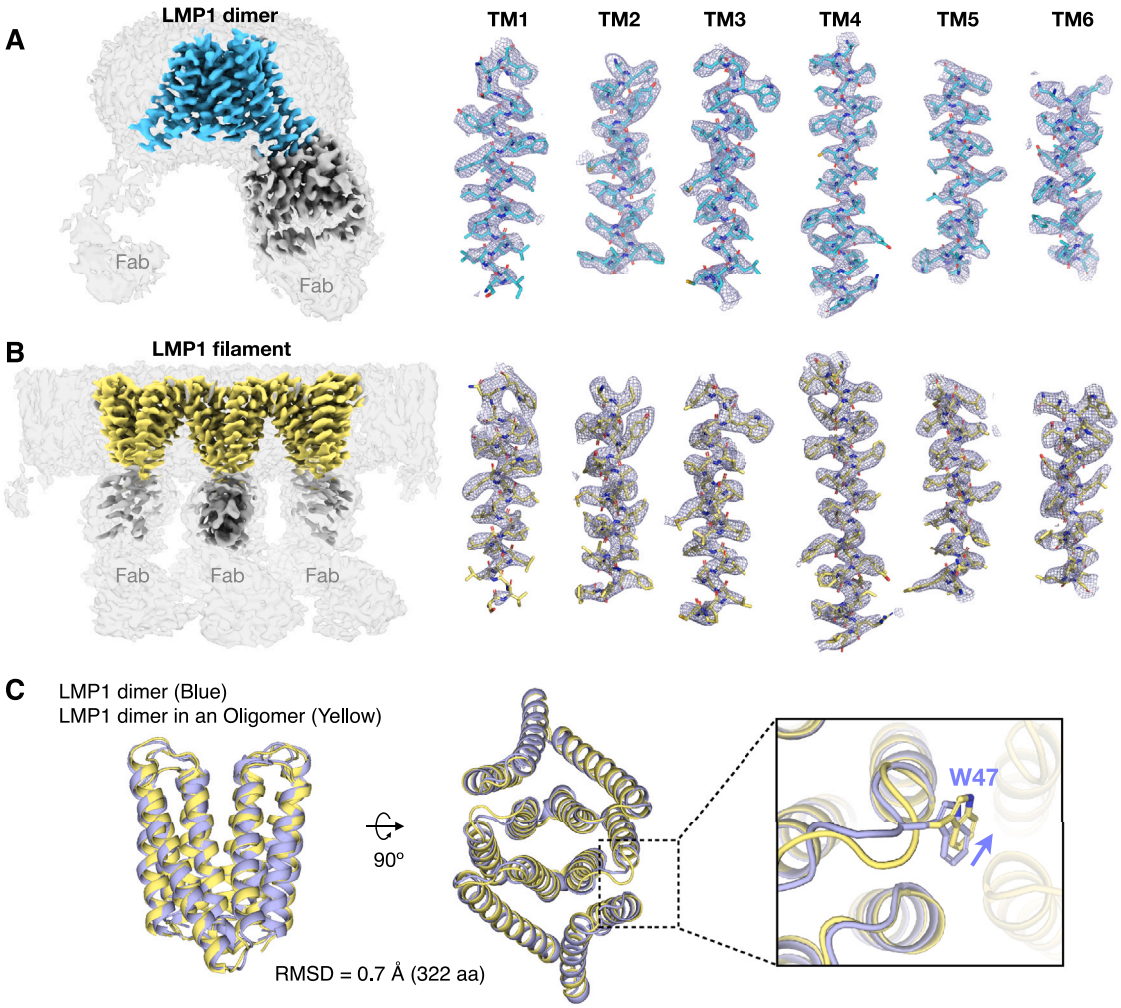

Figure S4. Cryo-EM density maps for LMP1 dimer and oligomer, related to Figures 1, 2, and 3

(A and B) Cryo-EM density maps for various parts of LMP1 dimer (A) and oligomer (B).

(C) Structure alignment of LMP1 dimer from LMP1 dimer (blue) and LMP1 dimer in an oligomer (yellow).

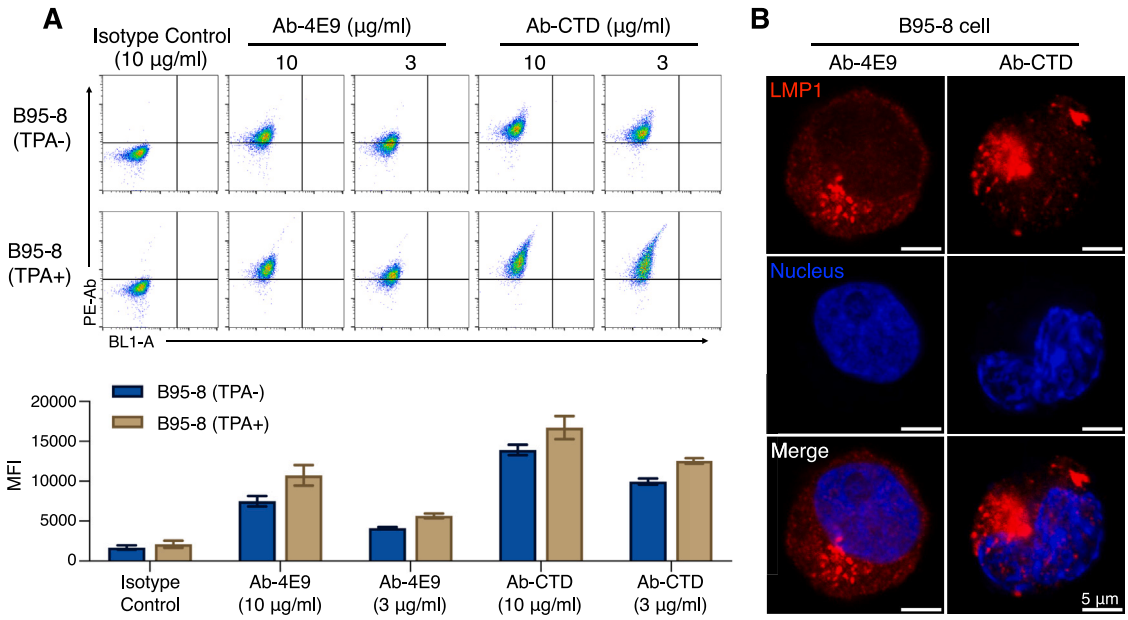

Figure S5. Antibody Ab-4E9 binds to endogenous LMP1 from B95-8 cells, related to Figure 1

(A) B95-8 cells, with or without induction by TPA, were stained with LMP1 Ab-4E9, Ab-CTD, or isotype control and PE-conjugated secondary antibody for flow cytometry analysis. Representative flow cytometry plots are shown in the upper panel, and median fluorescence intensities (MFIs) of three replicate wells from one of three independent experiments are shown in the lower panel. Data are represented as mean ± SD.

(B) Immunofluorescence staining of LMP1 Ab-4E9 (10 μg/mL) or Ab-CTD (3 μg/mL), TRITC-conjugated secondary antibody, and DAPI in B95-8 cells induced by TPA. Images are representative of three independent experiments. Scale bars, 5 μm.

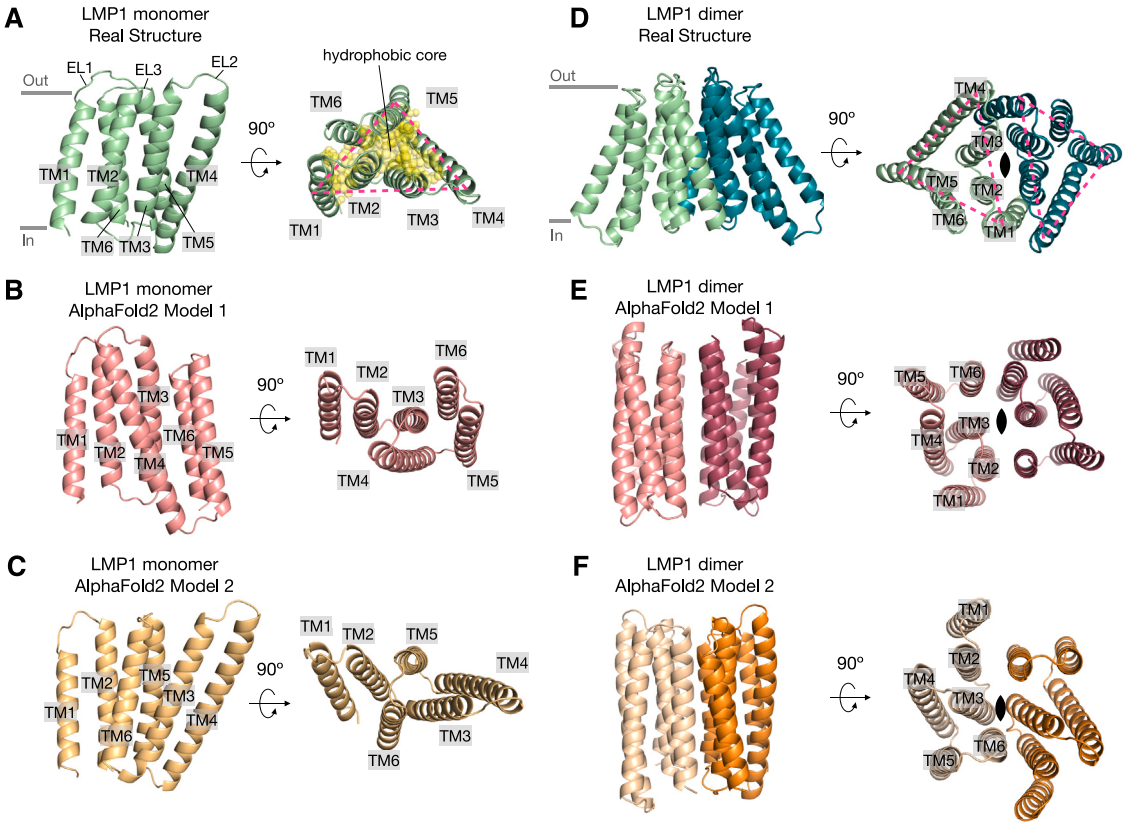

Figure S6. Comparison between AlphaFold2 predicted structures and experimentally determined structures, related to Figures 1 and 2

(A) Cryo-EM structure of LMP1 monomer in the side and top views. Hydrophobic residues facing the interior of the protein are shown in sphere representation and colored in yellow. EL, extracellular loop.

(B and C) The predicted models of LMP1 monomer by AlphaFold2 in the side and top views. The cryo-EM structure of LMP1 monomer (A) differs significantly from the predicted models by AlphaFold2 (B and C).

(D) Cryo-EM structure of LMP1 dimer in the side and top views.

(E and F) The predicted models of LMP1 dimer by AlphaFold2 in the side and top views. The cryo-EM structure of LMP1 dimer (D) differs significantly from the predicted models by AlphaFold2 (E and F).

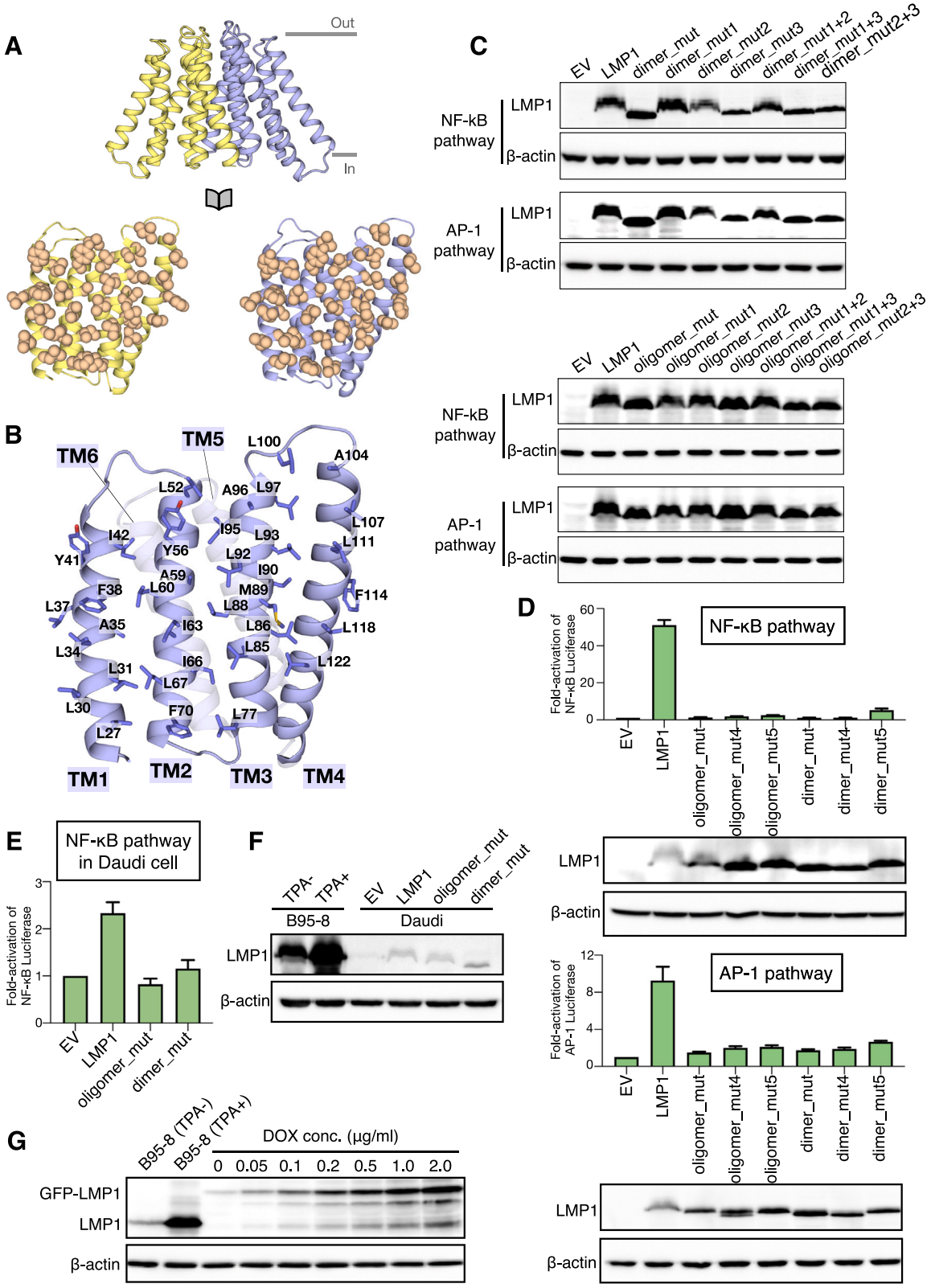

(legend on next page)

Figure S7. LMP1 dimer interface and mutants for LMP1 dimer and oligomer assemblies, related to Figures 2, 3, and 5

(A) LMP1 dimer is formed by a tight and antiparallel packing between the TM1/2/3/4 helices of each LMP1 monomer. Hydrophobic residues in the dimer interface are shown in sphere representation.

(B) A detailed list of key hydrophobic residues (shown in stick representation) distributed along the dimer interface.

(C) Expression levels of $LMP1^{fl}$ and different mutants in HEK293 cells. Cell lysates from equal numbers of different clones were immunoblotted for LMP1 and β-actin. β-actin was used as a loading control.

(D) Effects of $LMP1^{fl}$ mutations in the oligomer and dimer interface on LMP1-induced activation of the NF-κB and JNK/AP1 pathways in HEK293 cells. Averages and error bars of fold induction in luciferase assay are based on three independent experiments. Data are represented as mean ± SD.

(E) Effects of full-length wild-type LMP1, oligomer_mut, and dimer_mut on LMP1-induced activation of the NF-κB pathway in B lymphoblast Daudi cells. Averages and error bars of fold induction in luciferase assay are based on three independent experiments. Data are represented as mean ± SD.

(F) Immunoblot analysis of $LMP1^{fl}$ expression in the EBV-infected cell B95-8 and Daudi cells. TPA was used to induce EBV reactivation in B95-8. Cell lysates from equal numbers of different clones were immunoblotted for LMP1 and β-actin. β-actin was used as a loading control.

(G) Immunoblot analysis of $LMP1^{fl}$ expression in the EBV-infected cell B95-8 and HeLa cells. TPA was used to induce EBV reactivation in B95-8. HeLa cells were treated with different concentrations of doxycycline (DOX). Cell lysates from equal numbers of different clones were immunoblotted for LMP1 and β-actin. β-actin was used as a loading control.

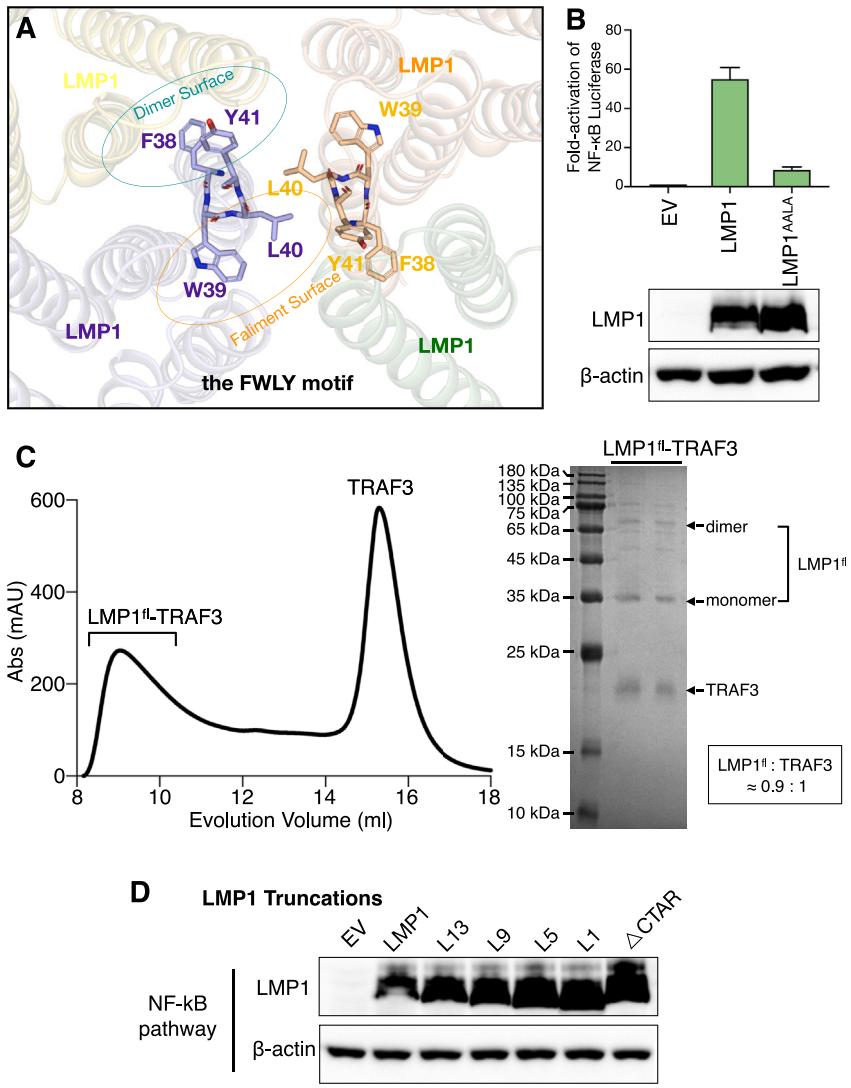

Figure S8. The FWLY motif contributes to LMP1 dimer and oligomer assemblies, related to Figures 4 and 6

(A) Detailed insights into the distribution of FWLY,[38–41] with F38 and Y41 buried in the dimer interface and W39 and L40 in the oligomer interface.

(B) Effects of the LMP1^{AALA} mutation on LMP1-induced activation of the NF-κB pathway. Averages and error bars of fold induction in luciferase assay are based on three independent experiments. Data are represented as mean ± SD.

(C) Size-exclusion chromatography of LMP1^{fl}-TRAF3 complex on a Superdex 200 Increase 10/300 GL column and the SDS-PAGE of the complex fraction.

(D) Expression levels of LMP1^{fl} and linker truncations in HEK293 cells. Cell lysates from equal numbers of different clones were immunoblotted for LMP1 and β-actin. β-actin was used as a loading control.